UNIVERSITY OF NAPLES FEDERICO II

DOCTORATE IN
MOLECULAR MEDICINE AND MEDICAL BIOTECHNOLOGY

XXXV CYCLE

Elvira Toscano

Modelling cultured cell migration and proliferation by integrating a phenomenological and a molecular approach

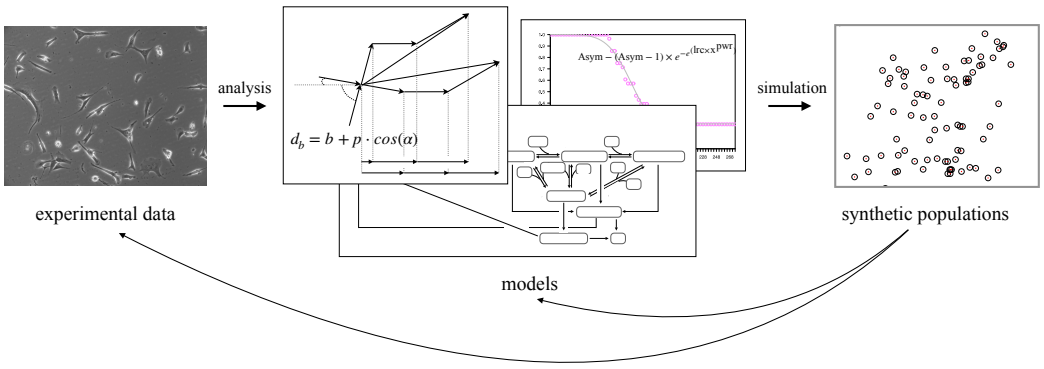

2019-2023

UNIVERSITY OF NAPLES FEDERICO II

DOCTORATE IN
MOLECULAR MEDICINE AND MEDICAL BIOTECHNOLOGY

XXXV CYCLE

Modelling cultured cell migration and proliferation by integrating a phenomenological and a molecular approach

Tutor
Prof. Giovanni Paolella

Candidate
Elvira Toscano

2019-2023

Table of contents

List of Abbreviations used

ODE - Ordinary Differential Equation

MSD - Mean Squared Displacement

SRW - simple random walk

CRW - correlated random walk

BRW - biased random walk

PDF - probability density function

Abstract

Cell cultures are a fundamental model system widely used to study the mechanisms involved in promoting and regulating cell proliferation and movement. Here we use a quantitative approach to study the behaviour of cultured cells by using models which reduce complex experimental observations to simpler systems, in which the contribution of different players may be more easily evaluated.

Following this approach, cell culture experiments were analysed by using a new motion model, developed to accurately evaluate cell migration features, such as randomness, persistence and directional bias, even when present in more complex combinations. The model was used to study the role of MAPK pathway in cell movement and to generate, within an in-house developed simulation tool, synthetic cell populations able to reproduce the same movement features. The simulation was later improved by pairing it with a biochemical simulator based on ordinary differential equations (ODE), which provided the ability to finely regulate the behaviour of synthetic cells according to the state of signalling pathways such as EGFR/ERK. In order to support the hour-long simulations needed to emulate cell cycle progression, several novel aspects had to be implemented, including synthesis and degradation of many proteins and a link between molecular pathways and cell mass and volume growth. To reproduce the delay, not easily obtained with ODEs, but typically introduced by gene transcription and mRNA translation, new modules were developed which attain this goal while maintaining a good balance between complexity and execution time, on one side, and manageability and accuracy, on the other. In its present state, the developed system reproduces different experimental situations and opens up future perspectives for further cell proliferation and movement studies.

1. Background

1.1. Studying the behaviour of cultured cells with quantitative models

Cell cultures are widely used in biomedical research and play a vital role in different research fields, such as biochemistry, cell and molecular biology, pharmacology, just to name a few. Biologists usually maintain cells as two-dimensional monolayer cultures, where populations composed of a single type or more complex mixtures are allowed to grow over a plastic or glass flat surface, submerged within a medium feeding the growing cells. Although conceptually simple and necessarily limited in their ability to reproduce the richer environment observed in vivo, cell cultures are widely regarded as extremely useful tools to understand cell biology, and have long been used to study cell movement, proliferation or growth in different experimental conditions, to investigate membrane, cytoskeleton or vesicular dynamics, to study the activation of molecular pathways and their influence on cell features and dynamics, just to name a few. Experiments performed on cultured cells are replicable, easily interpretable and considerably cheaper, when compared to other experimental systems, such as animal models, and in the last decades have been central to lots of findings as they reduce experimental complexity while keeping cells under tightly controlled experimental conditions that closely resemble their physiological environments.

While cell cultures have been studied and analyzed for a long time through different approaches and methods, the availability in more recent times of advanced imaging techniques and sophisticated labelling methods allowed quantitative analysis and dynamic observation of cultures at different time points to evaluate cell structures in relation to the presence of specific molecules, genome structure, gene expression. Real-time imaging techniques allow to follow cells over time to understand how they behave in time, how a

particular status is reached and how cells react to drugs or inhibitors added to the culture to interfere with their behaviour.

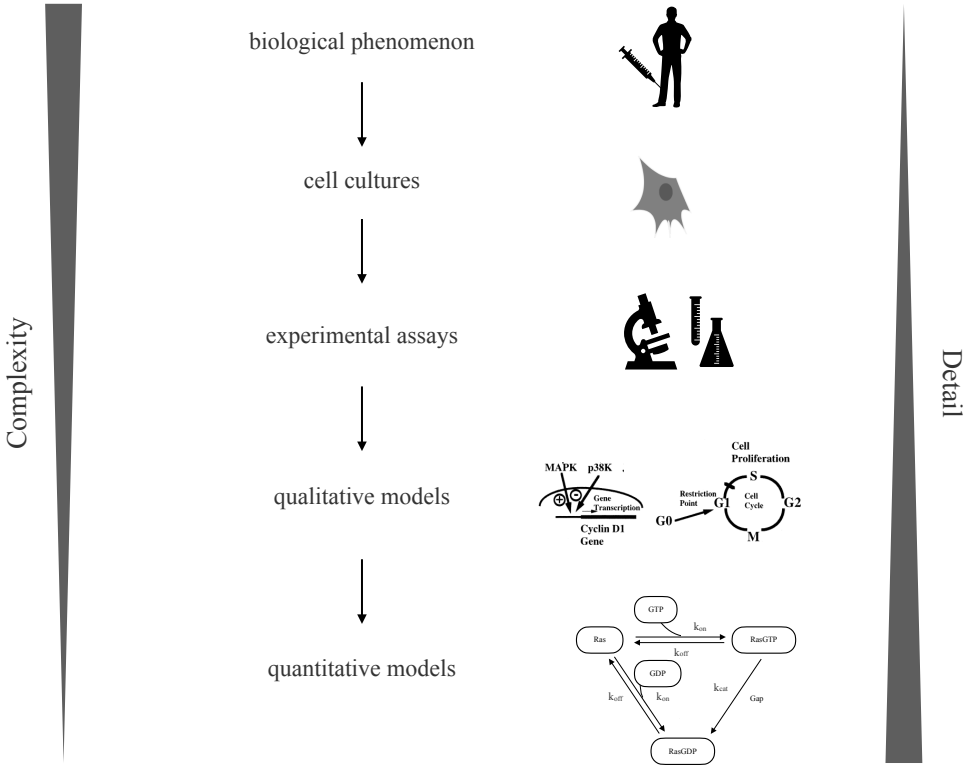

Figure 1. From qualitative to quantitative methods for studying cell culture behavior. Cell cultures, which are representations of a studied biological phenomenon, are used and studied with a variety of methods to reproduce easier environments to investigate and manipolate. From obtained data and observations, qualitative models are developed to describe observed dynamics and to formulate and verify hypotheses. Quantitative models allow to further reduce and dissect complexity of the studied phenomenon, in turn helping to increase detail in its knowledge.

Research using cell cultures has always been coupled to qualitative or semiquantitative models representing cell behaviour and/or intracellular molecular pathways. More recently, parameters descriptive of specific aspects of cell morphology and behaviour have been analysed by coupling dynamic microscopy with quantitative and statistical data analysis, to understand how the behaviour of a cell population changes over time and reacts to perturbations

(Figure 1). Mathematical models have often provided the opportunity to generate new insights, make testable predictions, verify gaps in knowledge, even test conditions that would be difficult to obtain with *in vitro* experiments on experimental cell cultures (Barh et al., 2020).

1.2. Cell attachment and growth

Cells seeded on a plate quickly attach and start growing. Cell adhesion depends on signals that also regulate differentiation, cell cycle, migration, and survival (Huang et al., 1999), and is essential in cell communication as well as development and maintenance of tissues. Changes in cell adhesion have been associated to a wide range of diseases including arthritis (Szekanecz et al., 2000), cancer (Huang et al., 1999; Okegawa et al., 2004, Hirohashi et al., 2003), osteoporosis (Perinpanayagam et al., 2001, Cho et al., 2006), and inflammatory diseases (Serhan et al., 2005; Simon et al., 2005). In vitro, when cells adhere to the surface of a culture flask or petri dish, they undergo morphologic alterations which imply deformation and reorganization of the cytoskeleton. The process is characterized by three stages: attachment to the substrate, flattening and spreading of the cell body, and organization of the actin skeleton with the formation of focal adhesions between cell and substrate (Khalili et al., 2015). Mammalian cells are often anchorage-dependent and attach firmly to the in vitro substrate (Sagvolden et al., 1999) and the better a cell sticks the greater is the number of chemical bonds with the substrate.

A fully spread cell starts increasing and modifying its volume and synthesizes proteins and other cellular components. Mass or volume changes in a given time interval are the combined consequence of protein biosynthesis (via transcription and translation) and mechanisms that add or remove cell mass via endo or exocytosis (Son et al., 2015) or volume changes determined by import of water driven by osmotic balance, hydrostatic pressure, and membrane

turnover (Cadart et al., 2019). Variability in growth can thus result from variability in either mechanism.

Typically, in mammalian cells, volume increase during the cell cycle shows little or no correlation to cell size at birth and different growth models have been proposed, exemplified by three simple limit cases: the *sizer*, the *adder* and the *timer*. In the first case, a size threshold (sizer) controls the entry into mitosis; this is the case, for example, of fission yeast, S. pombe, for which a perfect size control has been reported (Fantes et al., 1977). By contrast, an *adder* mechanism relies on the addition of a constant volume at each cell cycle that is independent of initial size, causing cells to converge on an average size after a few generations. This behavior has been also reported for several types of bacteria, cyanobacteria and in budding yeast (Campos et al., 2014; Taheri-Araghi et al., 2015; Yu et al., 2017; Deforet et al., 2015; Soifer et al., 2016). Finally, in the case of a *timer* mechanism, growth depends only on time: cells linearly grow by the same amount at each time interval (growth), therefore specific mechanisms should be required to maintain size homeostasis, or alternatively large cells would grow more than smaller ones and sizes would rapidly diverge, if cells just keep growing exponentially.

Mammalian cells have been hypothesized to control their size via a modulation of cell cycle duration. Specifically, an adaptation of G1 duration as a function of cell size has been proposed by a series of works (Dolznig et al., 2004; Ginzberg et al., 2018; Varsano et al., 2017). In HeLa cells it was found that, during most of the cell cycle, volume growth is nearly exponential with higher rates in S-G2 than in G1 (Cadart et al., 2022). HeLa cells were also shown to grow at a faster-than-average growth rate in G1 if they were born smaller than the others (Cadart et al., 2018) supporting the observation that inhibition of cell cycle progression has antagonistic effects on mass-specific

growth rate and, in turn, inhibition of growth pathways antagonizes cell cycle progression (Ginzberg et al., 2018).

1.3. Models for attachment and volumetric cell growth

Various attempts have been made to model processes involved in determining cell adaptation and spreading. A simple model describes contact area as increasing linearly with time, within the first 30-40 minutes of cell attachment, and later more slowly, to finally stabilise on a quite constant area value (Pietuch et al., 2013; Norman et al., 2010; Gauthier et al., 2009). This process is associated to an increase of plasma membrane area which varies according to cell type (Traynor and Kay, 2007; Boucrot and Kirchhausen, 2007; Gauthier et al., 2009).

The development of high-throughput single live cell imaging has provided a wealth of measurements which, in turn, promoted the development of models, aimed to quantitative characterization of cell growth and control of cell size. A set of growing complexity models developed to predict the dynamics of the average population behaviour was proposed by Mantzaris et al., 2007. Cells of an isogenic cell population have different sizes and volumes according to amounts of DNA, mRNA, proteins or metabolites and phenotypic cell-to-cell variability may originates from fundamentally different sources: unequal partitioning of cellular material at cell division and stochastic fluctuations associated with intracellular reactions. Assuming that heterogeneity originates from unequal partitioning at cell division, a deterministic cell population balance (DCPB) model was built, which predicts the entire distribution of phenotypes. In addition, a fully stochastic model accommodating both sources of population heterogeneity was developed using a novel Stochastic Variable Number Monte Carlo (SVNMC) algorithm, which incorporates all information included in the DCPB model but, in addition, accounts for intrinsic noise at the single-cell level originating from small

number of molecules and slow operator fluctuations. This model framework enabled the quantitative decomposition of the effects of the different population heterogeneity sources on system behavior indicating the importance of cell population heterogeneity in accurately predicting even average population properties (Mantzaris et al., 2007). More recently, a model able to characterize the joint correction of size by timing and growth rate modulation was developed. The model is based on three parameters: λ describes how the total relative growth depends on volume at birth ($log(V_{mitosis} / V_{birth})$), if λ is equal 1 the system behaves like a sizer, if it is 0.5 it is an adder and if it is 0 there is no size control at all; θ describes how cell cycle duration depends on volume at birth; γ describes the link between initial size and a variation in growth rate with respect to its mean value. By analyzing different cell types and different growth conditions, this model allowed to quantify the respective contributions of growth and time modulation to the effective size homeostasis behaviour allowing to highlight a common adder behaviour in cultured and primary cells (Cadart et al., 2018).

1.4. Cell movement

After attachment and spreading, typically a cell on culture dish is a dynamic entity, continuously changing its behaviour, position and shape, influenced by external stimuli and factors and itself influencing the surrounding environment. The movement of individual cells or cell groups from one location to another is referred to as cell migration and typically includes cell repolarization or reorientation in space, due to cytoskeletal reorganisation. Cell migration is involved in different fundamental processes, such as embryo development and organogenesis, organism growth and survival, and it can also be related to pathological conditions such as inflammation, atherosclerosis, tissue invasion by cancer cells and formation of tumor metastasis. On culture plates, cell movement depends on cell interaction

either with substrate and with other cells. In absence of particular conditions, cells move over smaller or larger distances, depending on cell type, and in all possible directions. Often they show a sort of inertia in their movement: at each time, they tend, at different extents, to maintain the direction of the previous motion step, as each change in direction would involve a membrane and cytoskeletal reorganisation and thus it would cost energy. Both in vivo and in vitro, cells are exposed to external stimuli which can affect their speed and direction; examples are chemotaxis or motion in presence of an inhibitor, a nutrient source, or a wound.

1.5. Mechanisms and molecules promoting cell movement

Cell migration studies have shown that morphological events are associated with changes at the ultrastructural and molecular level. Cell movement is the result of a highly coordinated process associated with polarization of the cell body according to an axis, typically oriented along the displacement direction.

The overall movement may be described as a cycle: a cell extends a protrusion at the leading edge; it establishes new adhesions with substratum at the front; then it performs a forward movement of its nucleus and body (traction); finally, it detaches the adhesions at the rear and retracts its tail.

Different studies implicate cell-substratum adhesiveness as an important determinant of cell migration speed, with maximum migration demonstrated at intermediate cell-substratum adhesiveness (Huttenlocher et al., 1996; DiMilla et al., 1993; Palecek et al., 1997). At lower substrate concentrations cell speed is apparently limited by the ability to form attachments at the cell front, whereas at high substrate concentrations cell speed tends to be limited by the rate of cell-substratum detachment. In fact, deadhesion/tail retraction may limit movement rate in strongly adhesive cells, such as cultured fibroblasts, which tend to have a strongly adherent, extended

tail and leave behind a trail of cytoplasmic fragments as they move. Instead, in weakly adhesive, fast moving cells such as amoebae and white blood cells, the tail is more rounded and this step is more efficient.

Cell movement involves assembly, disassembly or reorganization of actin cytoskeleton, and must be coordinated both in space and time to generate productive movement (Pollard and Borisy 2003). Actin filaments are double helical polymers of globular subunits all arranged head-to-tail to give the filament a molecular polarity where one end is called the barbed end (fast growing, or plus ends) and the other is pointed end. This polarity is key for actin assembly in cells. The actin cytoskeleton is important to stabilize the asymmetric distribution of key components of the directional response apparatus. In fact, during early events in polarization, filamentous F-actin changes its distribution losing the circular symmetry, around the cell rim, to concentrate in specific regions in preparation of the extension of protrusive structures which in turn are highly dynamic. These actin filaments are organized with their barbed ends preferentially oriented in the direction of the protrusion. The simplest structure they form are filopodia, which are thin cylinders that can extend tens of microns. Lamellipodia, instead, are thin protrusive sheets that dominate the leading edges of cultured fibroblasts and other motile cells. The characteristic rufflings at the fibroblast leading edges is due to lamellipodia that lift up off the substrate and move backwards (Mitchison et al., 1996).

Actin cytoskeleton, thanks also to a crosstalk with focal adhesion machinery, is involved in response to environmental cues. Focal adhesions are dot-like adhesion structures, located underneath the lamellipodium with the aim to sense the extracellular environment and thus affect their behaviour (Riveline et al., 2001). At the focal adhesion level, actin filaments can be linked to the cytoplasmic domains of integrin subunits through numerous anchoring

proteins, such as talin which is present at least in double copy connecting two integrin dimers with actin filaments (Geiger et al., 2009). These contacts are highly dynamic, in fact, during cell migration, both composition and morphology of the focal adhesion change: when a cell proceeds along its chosen path, a focal adhesion becomes progressively closer to the trailing edge and eventually must be dissolved to complete cell body translocation.

All the processes involved cell motility, including cell protrusion, cell retraction, cell-matrix adhesion, polarized exocytosis and polarized vesicle trafficking, are spatiotemporally controlled by various intracellular signalling pathways and by different intra/extra cellular factors.

Rho family GTPases (Cdc42, Rac, and Rho) are central regulators of cell migration, funneling signals from the cell environment to downstream components that shape cell motility. Cdc42 and Rac promote F-actin assembly and cell edge protrusion, whereas Rho facilitates myosin light chain (MLC) phosphorylation, activating myosin-based cell contraction. Rho is also a Rac antagonist and promotes F-actin polymerization through formins (Kühn and Geyer, 2014).

It is known that also calcium differential concentrations can modulated and influence cell migration. Interestingly, gradients in calcium concentrations with higher levels found at the cell rear have been seen in migrating cells and this asymmetry along with localized calcium fluctuations serves to regulate activation of different intracellular mediators, among which an attractive candidate for motion regulation is the calcium-dependent protease calpain. Calpain is a cysteine protease with two characterized isoforms, which localize to focal adhesions and cleave many focal adhesion related proteins including integrin receptors, talin, and focal adhesion kinase (Cooray et al., 1996; Huttenlocher et al., 1997). The increases in calcium seen in migrating cells appear to be within the range to support activation of calpain suggesting

that a reduction in calpain activity could inhibit cell migration by decreasing the rate of cell detachment and stabilizing integrin-cytoskeletal linkages.

Among the various intracellular signals that modulate cell motility processes, pathways downstream from Ras have been frequently involved, sometimes even cooperating with each other. Active PI3K has been implicated in the regulation of actin polymerization and formation of lamellipodia at the leading edge of the migrating cells, through its activity on the GTP-binding Rac protein. It was observed to be involved in controlling cell speed while directionality, more than speed, has been shown to be associated with MAPK pathway strictly depending on ERK phosphorylation (Sepe et al., 2013). ERK signalling, in fact, is considered one of the crucial regulators of cell movement, as supported also by findings that showed that the activated ERK localizes not only to the nucleus but also to cell protrusions and cell-matrix adhesion sites (Fincham et al., 2000; Stahle et al., 2003). Its role in the regulation of cell motility was initially revealed by experiments in which the activity or expression of MEK or ERK was modulated (Klemke et al., 1997; Krueger et al., 2001; Tanimura et al., 1998; Webb et al., 2000; Anand-Apte et al., 1997). On one hand, the role of ERK signalling in cell motility depends on its function in regulating gene expression. It promotes gene transcription of specific early and late responsive genes associated with lamellipodia extensions and tumor invasion and directly or indirectly modulates expression and function of SNAI2/Slug, TWIST1 and ZEB1/2, all factors driving epithelial to mesenchymal transition (EMT) reprogramming, thus inducing expression of pro-motile and pro-invasive genes (Chen et al., 2009; Hong et al., 2011; Ichikawa et al., 2015; Shin et al., 2010). On the other hand, ERK signalling regulates cell motility independently of its regulatory function on gene expression: ERK and RSK (a downstream kinase) directly phosphorylate various components that regulate cell protrusion and retraction, cell-matrix

adhesion and exocytosis necessary for coordinated cell motility. Among ERK substrates claimed to be responsible for ERK-induced peripheral effects, there are myosin light chain kinase (MLCK), involved in turnover of focal adhesions and extension of membrane protrusions (Klemke et al., 1997), and also Ca++-activated proteolytic enzyme calpain (Glading et al., 2004).

1.6. Methods and tools for studying cell migration

1.6.1.Experimental procedures and tools

Nowadays, a number of methods are used to evaluate the movement of cultured cells. The simpler approaches compare the final state or position with the initial, as for example in under agarose migration or Boyden chamber assays (Keenan et al., 2008; Pujic et al., 2009; Toetsch et al., 2009; Kim et al., 2012). The first consists of a layer of agarose gel put between the cell population and a chemoattractant source allowing chemoattractant diffusing in the gel and inducing cell migration into agarose. This system, first described in 1975 (Nelson et al., 1975), allows the use of multiple simultaneous chemotactic field. Variations to the method allow quantification of the number of cells migrating towards a particular chemoattractant: this was used to measure the number of migrating neutrophils in response to various manipulations (Heit et al., 2002). The Boyden chamber assay is commonly used as a migration assay, measuring the capacity of cells to move towards a chemoattractant gradient. The assay evaluates the movement of cells to the opposite side of a porous membrane also in response to chemoattractants (chemokines, growth factors, lipids or nucleotides) by quantifying the number of cells that appears in the lower chamber compared to the initial number in the upper chamber. Migration and invasion assays have been used, for example, to evaluate differential migratory ability following over-expression of a receptor (Castellone et al.,

2011) or to identify cell migration regulators, like small GTPases belonging to the Rho family (Hall, 2009).

Both methods do not allow direct observation of cell behaviour, so making it impossible to reliably discern between chemokinesis (general increase in migration in all directions) and directed migration of moving cells. The need for more in-depth characterization of the chemotactic response at the cellular and molecular level led to the development of assays for direct chemotaxis observation, also called bridge assays, such as Zigmond chemotaxis chamber (Zigmond et al., 1977) and its derivatives, Dunn (Zicha et al., 1991) and Insall chamber (Muinonen-Martin et al., 2010), or µ-Slide Chemotaxis (Zengel et al., 2011) that further improved the control and longevity of the gradient. These assays enable direct visualization of cells seeded in an observation area by forcing them through a bridge between two reservoirs filled with solutions of different chemoattractant concentration. Cells are exposed to gradients that are stable over 24 hours, thus meeting the requirements of studying chemotaxis of moving cells.

Time lapse microscopy provides great support for observing and studying the behaviour of eukaryotic cell cultures grown on plates under different conditions. Cells can be simply put, for example, in a small region of the plate and then observed while moving and diffusing in the free area. In other types of experiments, instead, cells can also be induced to a directional migration by specific stimuli, such as in wound healing assay. This technique exists in different variants: the wound can be created by using either a culture insert (cell exclusion assay) or more traditional strategies like a pipette tip (scratch assay). These methods have been widely applied to study cell migration. A scratch assay was used, for example, to show that wounds induced in Madin-Darby Canine Kidney (MDCK) cell sheets are closed by a crawling behaviour involving Rac, phosphoinositides and active movement of multiple

rows of cells (Fenteany et al., 2000). Wound healing assay has been also used to model the characteristic collective migration of L1 fibroblasts as a sheet migration and to identify the mechanisms that influence their spreading and migration as a group, while closing the empty area (Bindschadler et McGrath 2007). Overall, the technique results to be effective in analyzing cell migration, with some advantages and disadvantages specific for each case: the pipette tip scratch is a much cheaper and faster method while the culture insert yield more reliable and accurate results allowing the user to increase reproducibility between replicates (Pijuan et al., 2019).

1.6.2.Programs and tools for motion analysis

Computational methods and tools play an essential role in quantitative studies of cell migration by allowing to quickly analyze cell images or parameter files obtained from cell tracking. Several software packages have been developed, differently analysing cell motion parameters such as speed, motion persistence and directionality (Table 1) even though they often refer to them using different denominations and definitions.

As cell migration is a dynamic process, time-lapse microscopy experiments are usually designed to acquire images of moving cells over several hours. Image sequences are used to determine numerical features that then are processed through further analyses to give an interpretation of the observed behaviour. Many software tools track fluorescently labeled cells, usually easier to detect in comparison to cells acquired with other methods such as phase-contrast microscopy (Masuzzo et al., 2016).

Computational tools for cell motion analysis include commercial packages, like Imaris Track, MetaMorph and Image-Pro Plus (Web sites: Imaris Track; MetaMorph; Image-Pro Plus) as well as freely available tools. Some of them work as plugging within larger applications, such as in ImageJ: an example is MtrackJ (Web sites: MtrackJ), developed to facilitate manual

Method/Tool	Evaluated features			
	Displacement	**Speed**	**Persistence**	**Directionality**
AveMap	√	√	√	
Cell_motility		√	√	
CellMissy single-cell module	√	√	√	√
CellTrack	√	√		
CellTrackR	√	√	√	√
DIAS		√		√
Image-Pro Plus	√			
Imaris Track	√	√		
iTrack4U		√	√	√
MetaMorph	√	√		
MotoCell	√	√	√	√
Pathfinder		√	√	√

Table 1. List of free and commercial software packages evaluating cell movement. The table compares a set of existing softwares for cell migration analysis and lists evaluated cell movement features (as assessed from the online documentation provided by the software authors).

tracking of moving objects and used to evaluate cell displacement and velocity producing tracking data in a format that can also be read by other programs or Excel macros which typically allow the calculation of indices such as directional ratio, MSD (Mean Squared Displacement) and direction autocorrelation (Gorelik and Gautreau, 2014). iTrack4U is an automated cell tracking program, written in Java, which uses ImageJ as a library to track phase-contrast images (Debeir et al., 2005) and calculates total distance of migration, and the Euclidean distance between the start and end of the track and the persistence in cell movement direction (Cordelières et al., 2013). Another tool able to perform image analysis is DIAS (Dynamic image analysis system) which automatically detects the edge of the cells and computes the geometric centre (centroid) of each one at each time point. The position of the

cell centroid is then used to calculate parameters such as instantaneous velocity, direction of travel, direction change and the chemotactic index (Wessels et al., 2009). CellTrack is an integrated and extensible C++ software package for automated cell tracking and motility analysis (Sacan et al., 2008). A web application to study cell motility, MotoCell, has been developed in the hosting laboratory: it includes tools for image analyses, cell tracking and statistical analysis of cell behaviour that allow the evaluation of descriptive parameters calculated for the whole population as well as for each individual cell (Cantarella et al. 2009, Web sites: MotoCell). In the last decades, other image analysis tools were developed to analyze the movement of cells in particular experimental conditions. For example, TScratch is a freely available image analysis technique designed to automate the measurement of area progressively occupied by cells in wound healing assay (Geback et al., 2009). AveMap is a rapid, fully automated correlation-based method for cell migration analysis, compatible with standard video microscopy which, via an extensive dynamic mapping of cell displacements, allows for the computation of quantitative migration parameters, as cell motion velocity and persistence (Deforet et al. 2012).

Among the tools that perform analyses directly from cell tracking data and not form images there is Cell_Motility, which is an open source Java application, providing the user the MSD analysis with either overlapping or non-overlapping time intervals, as well as persistence time (the average time cell tends to maintain motion direction, see *Background* under 1.7.2) and cell motion speed (Martens et al. 2006). Other programs, such as Pathfinder, focus on migration of groups or clusters of cells. Pathfinder is a software capable of simultaneously measuring the migration speed, migration direction, and changes in migration directions of thousands of cells both instantaneously and over long period of time from fluorescence microscopy data (Chapnick et al.

2013). More recently, a new single-cell analysis module for CellMissy for cell migration data management was developed. The tool provides a powerful and largely automated pipeline for high-throughput, single-cell migration experiments downstream of image processing. It supports multi-parametric (speed, directionality), multiscale (step, trajectory), and quality-controlled analyses and allows fast comparison across the different tested conditions providing data visualization and assisted data filtering (Masuzzo et al. 2017). Very recently, an R package, celltrackR, was released, containing diverse state-of-the-art methods for both 2D and 3D cell tracks. It provides methods for data management, quality control, extracting and visualizing migration statistics, clustering tracks, and simulating cell migration. The package was specifically designed for immune cell migration data, but many of its methods can also be of use in other research areas dealing with moving objects. CelltrackR is compatible with migration data from any experiment using a standard format were the position of each cell is linked to the corresponding timepoint in time-lapse images. CelltrackR contains a range of motility statistics designed to characterize cell speed, straightness, and directionality. To help users exploring long-term effects of migration patterns *in silico*, celltrackR also implements three methods for simulating tracks: *bootstrapTrack* for sampling turning angles and displacements directly from a dataset, *brownianTrack* for simulating simple random walks, and *beaucheminTrack* for a random walk variation designed specifically for T cells (Wortel et al., 2021).

1.7. Models used to describe cell migration

Cell migration may be described as individual paths, each one composed by a number of segments, in which cells move in a straight line, joined by turning angles, at which cells decide whether to change direction or not. This decision is influenced by the current status of the cell and information coming from the surrounding environment. Cell movement is usually described

by using numerical parameters and mathematical models provide powerful options to better understand cell behaviour and to test hypotheses. Many movement models for cell migration are based on extensions of the simple diffusive model reproducing the irregular motion of individual pollen particles, famously studied by the botanist Brown, now known as Brownian motion.

1.7.1.Diffusive models

Eukaryotic cells growing on culture plates in standard conditions move in all possible directions travelling smaller or larger distances, depending on cell type. The diffusive model is possibly the simplest model used to describe cell movement and is based on the assumption that cells move freely without a preferential direction and the probability of changing direction is the same at each time. The diffusive model also implies that each movement is independent from that of the previous time steps, and that mean squared displacement (*MSD*) is proportional to elapsed time, according to a diffusion coefficient (*D*). This model is mostly accurate when suitably long observation times are used (Dunn and Brown, 1987; Gail and Boone, 1970). The diffusive model may be extended to include additional motion patterns by introducing new parameters according to the formula:

$$MSD = kt^{\alpha} \qquad (1)$$

where the α exponent is equal to 1 for a purely diffusive movement and the k parameter assumes different meanings for different α values, specifically for $\alpha=1$ $k=2dD$, where d is the number of dimensions, while for $\alpha=2$ $k=v^2$ as in uniform linear motion, where v represents the speed.

A diffusive behaviour can be obtained through a simple random walk (SRW) model. In a SRW, if we consider a one-dimensional movement, the probability density function (PDF) for the location of the walker after a time t is given by a Gaussian distribution:

$$p(x,t) = \frac{1}{\sqrt{4\pi D t}} e^{\frac{-x^2}{4Dt}} \quad (2)$$

where x is the walker position and D is the diffusion coefficient (Codling at al. 2008). In fact, if we suppose that the walker starts at the origin ($x=0$), after a time t it can move a distance d towards either left or right with a probability of 1/2 each. After a second time interval, the walker can be at a distance $2d$ to the left or right of the origin with a probability of 1/4 each, or it can be in the origin with a probability of 1/2. For large intervals, this converges to a normal distribution with a mean equal to 0.

The diffusive model has been found to well describe cell migration in conditions of loss of directionality induced by extracellular factors, such as the addition on plate of arachidonic acid. Arachidonic acid is an amphiphilic compound which goes into the cellular membrane, altering its composition and properties, and causing endothelial cells to lose their sense of direction and move having a diffusive behaviour. Arachidonic acid does not affect instantaneous speed of individual cells, but leads to a loss of ability for directed migration, in this case the mean squared displacement is found to be linearly related to time with a value of parameter α close to 1 (Rossen et al. 2011).

However, biological systems frequently exhibit a more complex behaviour. Many cell types move according to a model that is not simply diffusive, with *MSD* showing a non linear power-law relationship with time. Such situations are classified according to the value of α in the equation (1): for $\alpha<1$ we talk about subdiffusive movement, for $\alpha>1$ we refer to a superdiffusive movement, for $\alpha=2$ we have a ballistic diffusion, equivalent to moving in a straight line. Subdiffusive models accurately describe behaviour of migration paths in which the mean squared displacements increase more slowly than in a pure diffusive movement. This condition is a common feature of cells moving in confined environments, such as three-dimensional (3D) porous scaffolds,

hydrogel networks, and in vivo tissues. It has been found that movement of different cell lines in engineered biomaterial environments are well described by a subdiffusive model (Luzhansky et al. 2018). Conversely, cell migration on two-dimensional (2D) substrates, for example movement of cells cultured in a plate or cells living in unconstrained environments, is better described by superdiffusive models, among which we can find the persistent and biased models.

1.7.2.The persistence model

Cells do not move completely random but often follow persistent migration patterns, such as those produced by limiting the direction change in a random walk (Codling et al., 2008). This was observed in cultured cells in the seventies, when mouse fibroblasts were found to persist in their direction for about 2-3 hours (Gail and Boone, 1970). Years later, Selmeczi et al., by evaluating the parameters obtained from the model for both human fibroblasts and keratinocytes, proved that these cells appear to maintain memory of past movements (Selmeczi et al., 2005). Persistence is especially observed when movement is sampled at relatively short time periods, and appears as a sort of resistance to directional changes, possibly reflecting the need for membrane/ cytoskeletal reorganisation. Persistence seas not affect global direction of the movement, meaning that there is no overall preferred direction if movement is not otherwise biased. This feature, represented as a tendency to maintain, at each time step, the previous direction, has been variably referred to as persistence, linearity or sometimes also directionality, and differently measured in time units, i.e. how long the current direction influences the movement in subsequent time periods, or in terms of ratio between net displacement and length of the followed path (Deforet et al., 2012; Cordelières et al., 2013). There are, in fact, differences in the ways the different tools use to express and calculate parameters: what is called persistence within cAveMap (Deforet et al.

2012) and iTrack4U (Cordelières et al. 2013) in MotoCell (Cantarella et al. 2009) and CellMissy single-cell module (Masuzzo et al. 2017) is named linearity and end-point directionality ratio, respectively. Pathfinder (Chapnick et al. 2013) describes persistence in terms of the absolute angle of deflection, while in Cell_motility (Martens et al. 2006) and MotoCell persistence is expressed in time units and is calculated by fitting the model initially proposed by Fürth et al. in 1920 (Fürth et al., 1920) and described by Alt et al. in 1990 (Alt et al., 1990), where the relation between *MDS* and time (*t*) is given by the following equation:

$$MSD = 2S^2P\left[t - P\left(1 - e^{\frac{-t}{P}}\right)\right] \quad (3)$$

where *S* is the root mean squared speed and *P* is the directional persistence time, i.e. the time in which cell movement tends to persist in the same direction. For $t << P$, the displacement is determined by purely unidirectional motion and $MSD \sim S^2t^2$; whereas for $t >> P$, the movement is described by a normal diffusion and $MSD \sim 2S^2Pt$ (Dickinson and Tranquillo, 1993). This model is particularly effective in interpreting a wide range of superdiffusive motion patterns, starting from purely diffusive movement, with MSD proportional to time, up to movement along an almost straight line with MSD proportional to squared time as for uniform linear motion.

A persistent movement may be produced by correlated random walk (CRW), in which, at each time step *t*, each individual either changes direction and moves a distance *d* in this new direction, with a probability $p=\lambda t$, or moves a distance *d* in the previous direction, with a probability $q=1-\lambda t$. Hence, turning events occur as a Poisson process with rate λ (Codling at al. 2008).

1.7.3.Models for studying directionally biased cell migration

A superdiffusive movement may be also the effect of a superimposed directional bias, as, for example, in presence of a molecular gradient, generated

by a nutrient source, a chemical attractant, or even a wound inflicted to the cell layer. It may be modelled (Codling et al., 2008) as a factor altering diffusive movement by using the equation:

$$MSD = u^2t^2 + 2NDt \qquad (4)$$

where u is the speed increase over the purely random movement. In the case of biased movement, the walker has a higher probability of moving in the bias direction or close to it. This type of motion can be well described by the biased random walk (BRW). If we consider a one-dimensional movement, the probability density function for the location of the walker, performing a biased movement, after a time t is given by:

$$p(x,t) = \frac{1}{\sqrt{4\pi Dt}} e^{\frac{-(x-ut)^2}{4Dt}} \qquad (5)$$

where x is the walker position, D is the diffusion coefficient ad u is the velocity drift. This equation is similar to (2), except for drift term which shifts the centre of the Gaussian distribution from $x=0$ to $x=ut$. This distribution for a biased random walk in N dimensions becomes (Codling at al. 2008):

$$p(x,t) = \frac{1}{(4\pi Dt)^{N/2}} e^{\frac{-|x-ut|^2}{4Dt}} \qquad (6)$$

A feature of the biased model is the presence of a directional bias that may be estimated by analysing the probability distribution of movement directions in a circular plot. When the distribution is uniform, net displacements are distributed with equal probability F(θ) around the unit cycle. Instead the concentration of directions around a preferred one is well described by the Von Mises distribution:

$$f(\theta;\mu;\kappa) = \frac{e^{kcos(\theta-\mu)}}{2\pi I_0(\kappa)} \qquad (7)$$

where the parameter μ is the mean angle and the parameter k is the concentration parameter, where $k>=0$. The distribution is unimodal and symmetrical around $\theta=\mu$ (Bentley, 2006).

Despite the numerous tools available (Table 1), the calculation of persistence and directionality still creates problems when motion is affected by both, as for the eukaryotic cells moving under a directional stimulus: in this case the directional cell response affects the calculation, possibly generating wrong quantifications leading to misinterpretations of cells behaviour. This apparent confusion reflects the tight connection between directional persistence and directional bias: as both increase path linearity and each may influence the evaluation of the other one, wrong quantifications and misinterpretation of cell behaviour may easily occur (see also Table 2 in *Results* section) when, for example, cells move under a strong directional stimulus and both movement features are present at the same time.

1.8. Methods and procedures for studying cell proliferation

Cells on culture typically move and grow until they reach a particular moment of their life cycle when a *mother* cell proliferates giving rise to two *daughter* cells. Cell proliferation is involved in different fundamental processes, such as embryo development and organogenesis, or mechanisms of tissue repair and wound healing. This process is tightly controlled by genes and growth factors and typically is in equilibrium with mechanisms of cell death. When this equilibrium is altered or disrupted pathological situations can arise: an excessive and disordered of cell number characterizes neoplasia, while a slowdown in cell proliferation causes other types of diseases like degenerative diseases (Alzheimer or Parkinson disease).

Determination of cellular proliferation and population turnover is an important step for research on cell functions and is fundamental for understanding cell population dynamics and homeostasis. Historically this

study has been done by directly measuring DNA synthesis. Early studies employed incorporation of radiolabeled thymidine followed by autoradiography (Darzynkiewicz et al., 2011). Drawbacks of this method is obviously the use of radioactive substances and their disposal and its laboriousness and difficulty as an analysis of an high number of cells is required. Other methods which are routinely used for measuring cell proliferation include the use of BrdU (5-bromo-2-deoxyuridine), a halogenated thymidine analog labelling of newly formed DNA, which can be measured by flow cytometry detection using anti-BrdU antibodies (Dolbeare et al., 1983). An advantage of this method is that flow cytometry can be used to obtain both cell number as well as cell cycle information, however this method requires additional time and steps, expensive reagents and increased user-trained skills in order to operate the flow cytometer and analyze the resulting data. With some modifications, this approach has been used for the last 40 years to study proliferation dynamics of cell populations (Darzynkiewicz et al., 2011; Dolbeare et al., 1983). The method and timing of labeling depends on the experimental goals. For example, short term labeling identifies the proportion of cells actively replicating DNA during that period. When this approach is coupled with DNA content analysis, it provides a rich source of information about cellular proliferation. For example, the distribution of cells actively dividing according to their distribution in cell cycle phases or the number of resting cells can be easily calculated or information about the duration of DNA synthesis, doubling time, and cell cycle dynamics can be obtained. In spite of the widespread use of BrdU to measure DNA synthesis, this procedure includes relatively harsh fixation procedures and requires opening of the DNA using heat, acid or DNase to expose the BrdU epitope and allow access for anti-BrdU antibodies. These factors limit phenotypic analysis using antibodies directed to specific proteins due to destruction of epitopes and, additionally, variable

signal-to-noise ratios can also result from inconsistency in achieving exposure of the incorporated BrdU. To overcame these limits, a new flow cytometric method to label and detect nascent DNA using EdU (5-Ethynyl-2-deoxyuridine) has been developed and made commercially available (Salic et al., 2008). EdU, is a nucleoside analog of thymidine that is incorporated into DNA during S-phase just like BrdU and is not reactive in biological systems (Buck et al., 2008). EdU detection is based on an easily performed chemical reaction that does not require DNA denaturation, is quick and reproducible, and has a superior signal-to-noise ratio. This technique offers a wide range of opportunities to analyze cellular proliferation and population homeostasis (Flomerfelt and Gress, 2016).

However, there are also a range of other assays available for estimating dividing cells, each with varying levels of sensitivity, reproducibility and compatibility with high-throughput formatting. There are many direct and indirect methods of measuring cell proliferation of cultured cells in vitro which can be performed either as continuous measurements over time, or as endpoint assays. Among assays able to perform an indirect measure of proliferation there are methods which measure cell number (hemocytometer, cell imaging), or metabolic activity (luminescence-based assay). Conventional methods, as cell counting using a hemocytometer, are still useful. This assay is a low cost measure of the cell number; it quantitates an absolute cell count in cells/ml, requiring very little additional reagents or effort to prepare and run. However, there are serious disadvantages, which include the time consuming nature of the cell counting, high error rates that results in large standard deviations between counts, and the fact that a high range of cell numbers are necessary for accurate cell counts. These disadvantages make this method useful for cell counting of a small number of samples, and inadequate for larger high

throughput measurements where smaller plate sizes and lower seeding densities are required.

The need to perform measurements compatible with high-throughput formats has led to the development of multiwell-plate assays. The luminescence-based assays measure cell numbers based on a luminescent signal, by measuring the amount of ATP, which is proportional to the number of metabolically active cells. This is an endpoint measurement and once the reagent is added to the cells, the plate can only be quantified once. This simple method quantitates cell proliferation as a relative luminescence unit (RLU) using a reader plate. However, the reagent for this procedure have high cost and additionally the measurement is highly dependent on the metabolic activity of the cells. Various cell culture conditions, in fact, such as temperature or cell cycle time points, can readily affect the amount of ATP produced by the cells (Quent et al., 2010). Therefore, before starting with the measurements, it is important to control if the conditions of the experiment could interfere with the metabolic activity of the cells and potentially impede the relative luminescent signal generated by the cells.

Recently, the introduction of advanced cell imaging platforms has allowed for new tools which monitor cell proliferation while providing quantitative and qualitative phenotypic data collection. Thanks to these methods based on observations of cell cultures with microscopes, mitotic cells can be identified by simply counting cytokineses or by using particular antibodies and staining. Fluorescent molecules able to bind DNA are typically used and can reveal chromosome condensation state; alternatively antibodies specifically recognizing microtubules are used to reveal mitotic spindle formation. Imaging methods provide avenues to measure cell proliferation, either by continuous measurement or endpoint assays. It has high-throughput capabilities as it can be automated to capture multiple images for each well, in

real-time along with temperature control, using the same cells over the duration of the assay. The software accompanying the cell imaging devices allow for the quantitation of cell counts using the different parameters even though sometimes they are limited in the ability to split touching objects. Overall, these methods are a significant improvement on the conventional hemocytometer cell counting method and are a more cost effective option to the luminescence-based assay (Morten et al., 2016).

1.9. Models for cell proliferation

Cell populations show different proliferation patterns according to cell type or different environmental conditions. There are several mathematical models that in the years have been developed for studying cell proliferation; some of them have been applied in the prediction of different biological phenomena, for example growth speed of a cancer mass and definition of an appropriate therapy.

Under ideal conditions, a cell population typically grows following an exponential pattern. The exponential model of Malthus (Malthus, 1798) is one of the first models introduced for studying population growth; it is based on the fact that the increasing of number of entities in a time unit is proportional to population dimension at the start of each observation time. According to this model, the number of entities *x(t)* is given by the following formula:

$$x(t) = x_i e^{at} \quad (8)$$

where x_i is the starting number, t is the time, and a is the growth rate ($a = \frac{1}{x}\frac{dx}{dt}$) which in the Malthus models is assumed to be constant. The exponential model well describes different experimental conditions, but, being based on the assumption that the growth rate is constant in time, it produces non optimal results and is too restrictive for example in situations in which lags at the start and/or at the end of the observation time are present.

To overcome these limits and to allow an accurate description of a higher number of cases, other models have been introduced. Gompertz model (Gompertz, 1825) tries to overcome these limits by assuming that growth rate decreases exponentially with time; in this way, it is able to follow also situations in which are present environmental difficulties arising with population growth, like nutrients or space loss. In this models the number of entities *x(t)* as function of time *t* is given by the equation:

$$x(t) = M\ e^{-e^{-k(t-t_m)}} \quad (9)$$

where *M* indicates the maximum value or higher asymptote, and *k* is a constant that determines the curvature of the growth pattern and t_m is the inflection point at which the growth rate reaches its maximum value. The equation (9) describes an asymmetric curve which predicts that at the time of inflection t_m, *x(t)* is equal to *M/e.*

The logistic model, introduced by Pierre F. Verhulst in 1838 (Verhulst, 1838), instead, implies that the growth rate decreased in time according to population growth. In this case, the described curve is symmetric is given by the equation around the point of maximum growth (point at which x(t) becomes equal to M/2) and is given by the following equation:

$$x(t) = \frac{M}{1 + e^{-k(t-t_m)}} \quad (10)$$

A generalization of the logistic model is the more flexible Richards model (Richards, 1959), which introduced a new parameter *v* in the equation to deal with asymmetrical growth:

$$x(t) = \frac{M}{(1 + v\ e^{-k(t-t_m)})^{1/v}} \quad (11)$$

The need for a more flexible model, which could be successfully applied in a higher number of situations, leaded to the introduction of other curves, like that developed by Waloddi Weibull in 1951 (Weibull, 1951). This

curve, initially developed for describing file cycle of industrial products, well models situations in which the growth rate is proportional to time up to a factor indicating the shape of the curve *k*:

$$x(t) = 1 - e^{\frac{t}{\lambda}^k} \qquad (12)$$

where λ indicates the scale, which is the time at which the 63.2% of observed events have occurred. A *k* value equals to 1 reduces Weibull curve to an exponential one: in this sense, the exponential curve can be considered a particular case of Weibull curve.

Function (12) can be also written including the asymptote *M*:

$$x(t) = M - De^{-ct^k} \quad (13)$$

where *D* is the difference between final and starting values and *c* is a constant ($c = 1/\lambda$). These parameters give flexibility to the curve which becomes able to well describe the proliferative behaviour of different cell populations also in different experimental conditions.

1.10. Cell cycle progression and regulation

Cellular molecular mechanisms that rule cell proliferation and cell cycle progression are highly complex and their understanding has grown rapidly as, over the years, research groups around the world have deeply explored the intricate details of Cdks implicated in cell cycle and their associated activators and inhibitors (Bartek et al., 1996; Sherr, 1996; Sherr and Roberts, 1999; Cross and Roberts, 2001).

Cell cycle consists of oscillating changes in protein concentrations and activities within the cell allowing for duplication of the genome and cell division. This process is highly regulated involving multiple cellular mechanisms including oscillating changes in protein expressions regulated at the transcriptional and post-transcriptional levels, changes in post-translational modifications and functional activities, and changes in protein-protein

interactions and subcellular localizations (Lindqvist et al., 2009; Pines et al., 2011; Davey et al., 2016). Alteration in any one of these events can result in changes in the dynamics of each relationship, and ultimately in the cell cycle dysregulation, a hallmark of several diseases, like cancer or viral infections.

Several control mechanisms ensure that each chromosomal DNA sequence is replicated once, and only once, during a specific time window, the S-phase. Following S-phase, replicated chromosomes separate during mitosis (M-phase) and segregate in two nuclei that are then endowed to two newborn cells at division. Two gap phases, called G1 and G2, separate cell birth from S-phase and S-phase from M-phase, respectively.

If growth factors are absent or low, cells which are in early G1 phase leave the cycle and enter a reversible resting/quiescent state referred to as G0 (Coller et al., 2006; Iyer et al., 1999) while older cells finish the ongoing cycle and enter the resting state after mitosis. A relevant regulatory step is at G0/G1 transition, a point called restriction (R) point where intracellular and extracellular signals are monitored and integrated (Pardee et al., 1974; Pardee, 1989; Bartek et al., 1996; Planas-Silva and Weinberg, 1997). Upon growth factor refeeding, signal transduction pathways are activated, ultimately leading to S-phase onset. Quiescent cells, before reaching the R point, need continual feeding of nutrients, mitogens and survival factors; in contrast, past the R point, they are irrevocably committed to divide independently from the continuous presence of growth factors in the medium (Pardee et al., 1989). The restriction point R operates stringently in normal cells, but it is defective in cancer cells that accumulate mutations, typically in proto-oncogenes or tumor suppressor genes, resulting in constitutive mitogenic signaling and defective responses to anti-mitogenic signals that contribute to unscheduled proliferation (David-Pfeuty et al., 2006; Malumbres et al., 2004; Massagué et al. 2004).

Growth factors bind to specific receptors in the plasma membrane, stimulating an intracellular signaling, like through the Ras–Raf–MAP kinase pathway, that activates a cell response. Among the genes whose expression is induced there are D-type cyclins (Sherr, 1995; Bartek et al., 1996) which, combined with Cdk4 and Cdk6, set in motion the cell-cycle engine that drives rounds of DNA replication, mitosis and cell division. CycD/Cdk4 stimulates cell growth and division by phosphorylating the retinoblastoma protein, Rb (Weinberg, 1995; Planas-Silva and Weinberg, 1997), which is a specific inhibitor of E2F, a transcription factor for the CycA and CycE genes (Bartek et al., 1996; DeGregori, 2002). Rb, once hyper-phosphorylated by CycE/Cdk2, releases its hold on E2F, which, in turn, stimulates synthesis of CycA and CycE. Because these cyclins, in combination with Cdk2, can phosphorylate Rb (Planas-Silva and Weinberg, 1997), CycA and CycE activate their own synthesis. Dephosphorylation of Rb is catalysed by a type-1 protein phosphatase (PP1), whose activity is inhibited by cyclin/Cdk complexes (Dohadwala et al., 1994; Kwon et al., 1997). PP1 phosphorylation is started by CycE/Cdk2, with CycA/Cdk2 and CycB/Cdk1 keeping PP1 phosphorylated until the end of mitosis (Mittnacht, 1998). Another role of Rb is to repress the transcription of housekeeping genes by inhibiting RNA polymerases I and III (White, 1997). By this mechanism, Rb interferes with general cell growth as well as the synthesis of E2F specific gene products. An inhibitor of cyclin activity is p27Kip1, which binds to CycA/Cdk2 and CycE/Cdk2 dimers to form inactive trimers (Sherr and Roberts, 1999). In turn, phosphorylation of Kip1, catalysed by Cdk complexed with CycA, CycE or CycB, promotes Kip1 ubiquitination (Sheaff et al., 1997; Vlach et al., 1997) and degradation by a protein complex called the SCF (Amati and Vlach, 1999). Clearly, Kip1 and the CycA- and CycE-complexes are mutual antagonists: either Kip1 is

abundant and the cyclins are inactive, or Kip1 is absent and at least one of the cyclins is active.

As CycA rises, it initiates DNA synthesis. Normal cell implements an advanced system which transduces DNA damage signal to a regulatory mechanism of the cell cycle and arrests the cell cycle progression (Dasika et al., 1999). According to this system, DNA damage activates tumor suppressor gene p53 which activates Mdm2 and p21 sequentially. The latter binds the binary complexes Cyc/CDK forming a trimeric complexes p21/Cyc/CDK which disturb the cell cycle progression. Moreover, p53 induces a repair mechanism of DNA damage activating other pathways related to conservation of genetic code (Shu et al., 2007), thus playing an important role in the protection system which maintains the stability of cell cycle.

The end of DNA synthesis allows starting accumulation of CycB, so that the cell can be able to enter mitosis which is the final stage of the cell cycle resulting in cytokinesis and cell separation. This unidirectional process is centered upon activation and then inactivation of the CycB/CDK1 complex (Lindqvist et al., 2009). The complex formation is initiated in the G2 phase by increasing steady state levels of CycB, dynamic changing in phosphorylation status, and relocating numerous proteins. Modification by WEE1 proteins disrupts the complex kinase activity while dephosphorylation of the complex is mediated CDC25 proteins. Activities of both WEE1 and CDC25 enzymes are also tightly regulated. Their regulators include Polo-like kinase 1 (PLK1) and several phosphatases (PPase) such as Protein phosphatase 2A (PP2A) (Gheghiani et al., 2017; Ovejero et al., 2012; Potapova et al., 2011; Forester et al., 2007). Moreover, positive feedback by the active complex CycB/CDK contributes to further WEE1 inactivation and CDC25 activation. Upon reaching a threshold level, active complex initiates nuclear envelope

breakdown (NEBD), spindle formation, and chromatin condensation by phosphorylating diverse targets.

Transition through mitosis involves activation of the E3 ubiquitin-protein ligase complex known as Anaphase-promoting complex or cyclosome (APC/C) (Pines et al., 2011; Davey et al., 2016; Castro et al, 2005; de Boer et al., 2016) which initiates CycB degradation by ubiquitinating and targeting it for proteolysis by proteasomes (Morgan, 1999). APC-dependent degradation of mitotic cyclins is mediated by adaptors, Cdc20 and Cdh1 (Morgan, 1999; Zachariae and Nasmyth, 1999) which are regulated differently during the cell cycle thanks the phosphorylation by CycB/Cdk1, PLK1, MCC (Mitotic Checkpoint Complex) and dephosphorylation by PP2A. When APC/C:CDC20 ubiquitin ligase complex becomes active, targets for degradation CycB and Securin, which prevents sister chromatid separation by the enzyme Separase. Upon activation of the APC/C:CDH1 ubiquitin ligase complex, mitotic exit is initiated by degradation of substrates including CDC20, PLK1, and any remaining CycB.

1.11. Biochemical models of cell cycle progression

Cell cycle has been the target of many molecular models which try to reproduce the cycle, in part or in full, by using ordinary differential equations for simulating small or large numbers of cell cycle reactions. Considering the large number of molecular species and reactions involved and the additional problem of expressing genes in a coordinated way, many of them tend to focus on specific events and/or checkpoints with different levels of detail.

One of the first cell cycle models was developed by representing transitions between the cycle phases as first order processes in a system of ordinary nonlinear differential equations. The model also includes the resting state (G_0) from which cells could reenter the reproductive cycle in response to a growth regulatory substance (Piantadosi et al., 1983). Similarly, very simple

models have been proposed in the following years, aimed to investigate the role of differs molecules on cell cycle progression. In 2012, a mathematical model was proposed, by connecting the dynamics of glucose and insulin with the β-cell cycle by using a system of ordinary differential equations. The model showed how glucose and insulin concentrations modify the transition rate from G1- to S-phase. Similarly to the previous model (Piantadosi et al., 1983), the evolution of cell cycle was simulated as very simple phase transitions. The model allowed representing different pathological scenarios (type 1 or type 2 diabetes) and reproducing the behavior of the glucose-insulin regulatory system showed in biological experiments (Gallenberger et a., 2012).

More complex models have been often based on simpler ones which simulate dynamics typical of simpler organisms like yeast. The main elements of signaling of the full cell cycle were included in a model in 2004, where a set of nonlinear differential equations was used to represent the physiological responses of mammalian cells to transient inhibition of growth (Novák and Tyson, 2004). The model relies on a previous work on the regulation of cyclin-dependent protein kinases during the cell division cycle of yeast (Chen et al., 2000) which was supplemented with equations describing the effects of retinoblastoma protein on cell growth and the synthesis of cyclins A and E, and with a representation of the signaling pathway that controls synthesis of cyclin D. The model emphasizes the deep similarities of the Cdk-regulatory systems in yeast and mammalian cells and was based on the idea that G1 events are driven by the switching properties of positive-feedback loops and antagonistic interactions. It was subsequently included, with other models, into a generic model for the regulation of DNA synthesis and mitosis with the aim of emphasizing the universality of the regulatory system among eukaryotic cells (budding yeast, fission yeast, frog eggs, and mammalian cells) (Csikasz-Nagy et al., 2006).

However, nowadays, most models are not intended to account for all aspects of the intricate regulation of the mammalian cell cycle: to reduce complexity and generate experimentally tractable predictions, they focus on a particular stage of cell cycle and on its regulation, without arriving to final cell division readout. Different mathematical models, specifically focusing on the G1 to S transition in the mammalian cells, have been reported (Aguda et al., 1999; Qu et al., 2003; Swat et al., 2004; Haberichter et al., 2007; Kohn et al., 1998) and each one uses a specific approach and/or focuses on specific components to simulate the cell cycle dynamics. These include models whose core module is the E2F-pRb complex (Kohn et al., 1998; Yao et al., 2008); restriction point models involving D-type and E-type cyclins, their kinases Cdk4 and Cdk2 and the inhibitors (Aguda et al., 1999); models considering multiple phosphorylation sites for the components involved in the regulation of the G1 to S transition (Qu et al., 2003); models considering only few components in the G1/S transition but aimed to identify the small feedback loops in the regulation process of the restriction point transition (Swat et al., 2004); models based on the presence of metabolically responsive modifiers (Haberichter et al., 2007). In 2009, a mathematical model of the G1/S networks was developed by using, as in the previously described model (Novák and Tyson, 2004), a model representing the G1/S transition in budding yeast (Barberis et al., 2007). The major element of novelty of this new model was the inclusion of localization and compartmentalization of key cell cycle players, and the modeling of cytoplasmic/nuclear shuttling of cyclins, cyclin-dependent kinases, their inhibitor and complexes. The model was implemented using ordinary differential equations (ODE) and allowed to identify the molecular mechanism that underlies the restriction point, yielding specific predictions and giving new insights on the role that the availability of Cki would have on the entrance into S phase (Alfieri et al., 2009). An integration of a G1/S checkpoint

model (Tashima et al., 2004) with a signal transduction of DNA damage model (Lev Bar-Or et al., 2000) was proposed in 2008 (Iwamoto et al., 2008). It was represented by 28 ordinary differential equations including 75 kinetic parameters and simulated the interaction between Cyc/CDK and Rb/E2F cycle, the oscillation of p53, the delay of the cell cycle progression with occurring DNA-damage and the expression of p21 corresponding to the intensity of DNA-damage.

Other models, instead, focus on representing the mitotic phase. The initial models on CycB/CDK kinase activation and feedback regulations by WEE1 and CDC25 (Goldbeter et al., 1991; Tyson et al., 1991; Novak et al., 1993; Sible et al., 2007; Gerard et al., 2013; Verdugo et al., 2013) determined that the relationships act as a bistable on/off switch, committing cells to mitotic entry. More recently, by using a combination of previously published kinetic parameter values and analysis of qualitative and quantitative experimental data, a novel computational model of cell mitosis was developed for the purpose of generating new hypotheses and predicting new experiments designed to help understand complex diseases (Terhune et al., 2020). The new model is based on a hybrid framework combining Michaelis-Menten and mass action kinetics for the mitotic interacting reactions. The model starts at mitotic entry initiated by the activities of CDK1 and PLK1, simulates reactions involving APC/C bound to CDC20, and ends upon mitotic exit mediated by APC/C bound to CDH1. It includes syntheses and multiple mechanisms of degradations of the mitotic proteins. This newly constructed model was used to provide insights into the dysregulation and pseudo-cycle creation required for successful infection of a human herpesvirus, cytomegalovirus (HCMV). By simulating infection of the cytomegalovirus, the model was used to hypothesize that virus-mediated disruption of APC/C was necessary to establish a unique mitotic collapse with sustained CDK1 activity. This model was then extended including crosstalk

between Plk1, p53, and G2/M DNA damage checkpoint (Jung et al., 2021). The new developed model was used to analyze the cancer cell cycle progression under various gene perturbations including Plk1 depletion conditions. Mutations and perturbations in approximately 1800 different cell lines were analysed and the model was able to successfully explain phenotypes of the different cancer cell lines under different gene perturbations. While the Plk1 and p53 pathways are often studied independently, this model allowed to study the crosstalk between these pathways and their individual and cooperative regulatory functions.

2. Aims

The aim of this work was to understand physical and chemical rules and constrains affecting movement, growth and replication of cultured cells, observed at different levels including morphological changes, biochemical pathways and chemical reactions. Overall, this approach implied the dissection of complex experimental observations into more simple interacting systems where the contribution of different players are separately evaluated and modelled.

It was chosen to use an approach based on analysing and reproducing the behaviour of laboratory cell cultures observed in time lapse microscopy, in which cells from specific lineages are grown under different conditions. An important point was to take into account cell appearance as well as its biochemical and molecular status.

In order to reach this goal, a basic requirement was the development of mathematical models able to describe movement and proliferation of individual cells grown as an experimental culture, to be used to extract features and parameters characterising the different processes. A central step in this plan was the set up of a simulator, which, by using such models, could be used to create novel cell populations *in silico,* which accurately reproduce the experimental population from which the model parameters were originally derived. A distinguishing feature was that biochemical models be used to control the simulations, by calculating molecular levels of activators or other regulatory proteins, according to cell condition, time and position and to use these levels to accordingly influence the stochastic simulation.

3. Material and Methods

3.1. Cell culture

Cells were grown in 100 mm diameter Petri plates in Dulbecco's Modified Eagle's Medium (DMEM) supplemented with 10% fetal bovine serum (FBS), penicillin (10 U/ml), streptomycin (10 ng/ml) and L-Glutamine (2mM) and maintained in incubator at 37°C and with atmosphere made up to 95% air and 5% CO2. Cell propagation was performed by detaching cells with a solution of trypsin/EDTA (trypsin 0.05% and 0.53 mM EDTA) and collecting them with complete culture medium. After centrifugation at 1200 rpm for 5 minutes, pellets were suspended in fresh medium, properly diluted, and plated again.

The cell lines used for time lapse acquisitions include murine fibroblasts NIH-3T3 (Todaro et al., 1963) and NIH-Ras produced by transfecting RasV12 into NIH-3T3 (Sepe et al., 2013), and human immortalized cell lines HeLa from cervical cancer (Gey et al., 1952), T24 from bladder carcinoma (Bubeník et al., 1973) and MDA-MB-231 from breast cancer (Cailleau et al., 1974).

To investigate random movement ability, 25000 cells/well were seeded in 12 well plates and maintained in complete medium at 37°C in an incubator with 5% CO2. After 16-18 hours, the plate was placed in the incubator chamber of the microscope. For wound healing assays, cells were seeded in confluent monolayers by plating 250000 cell/well in 12 well plates in complete medium; 24 hours after plating the cell layer was scratched with sterile pipette tip.

To study the role of specific molecules in the migration process, some of them have been targeted by using inhibitors. PD98059 (2'-Amino-3'-methoxyflavone) was chosen as selective and cell-permeable inhibitor of MAP kinase kinase (MEK1/2); it is a non-ATP competitor that binds to the inactive

form of MAPKK and prevents its activation by upstream activators and subsequent phosphorylation of downstream substrates. FR180204 (5-(2-Phenyl-pyrazolo[1,5-a]pyridin-3-yl)-1H-pyrazolo[3,4-c]pyridazin-3-ylamine) was used to block ERK1/ERK2; it acts as a competitive inhibitor which interacts with ATP binding domain. Starting from stock solutions prepared by dissolving each inhibitor in DMSO, PD98059 was used at final concentration of 40 μM and FR180204 3mM.

3.2. Data acquisition

Phase contrast images (objective 10x) of different samples have been acquired every 10 minutes for 24 hours by using *PhotoCell*, a set of macro tools developed to manage time-lapse acquisitions (see *Appendix*, under 10.1), and by taking the advantages of Zeiss Cell Observer system composed by an inverted microscope (Axiovert 200M), an incubator chamber that maintains the temperature at 37°C and CO2 pressure at 5%, and a digital camera. A motorised stage along the three axes permits prolonged automatic acquisitions at different positions. For this work, digital frames were acquired as 8 bit images of 650x514 pixels. The pixel scale of the acquired images is 0.767 pixel/μm, obtained by acquiring with the same system an image of a Burker chamber with known measures.

Cell displacement was tracked by using a semi-automated procedure available within MotoCell (Cantarella et al. 2009). The tracking procedure allows to collect cell positions (in terms of x/y coordinates) at different times (frames) to construct the entire path of each cell that is characterised by an origin (start, newborn, found, gone in) and a destiny (split, dead, lost, gone out). The registered data are written and stored in a text file that can be read by MotoCell to perform the quantitative analysis.

3.3. Software and languages

Computational tools developed for this work have been built by using different languages and systems. PHP (Web sites: php) is the main programming language used for the development of the different MotoCell modules. It is a scripting language tightly integrated with the Apache web server as it was originally designed for producing dynamic web pages; within this work, it is has been widely used to implement procedures and tools by taking advantage of its C-like syntax combined to rapid execution and testing and of the object-oriented programming (OOP) paradigm, which allows single program entities to interact with each other while keeping their own properties and functions separated. The OOP approach allowed the development of strongly modular programs, where different tools share the same objects and thus acquire common as well as specific features and behaviour.

Most development was done within the environment provided by MotoCell (Cantarella et al. 2009), a PHP web application, which provided a easy development environment where to test new models and procedures while taking advantage of a large library of cell motility analysis tools, the ability to integrate new modules in the form of *analyser* objects and rapid production of complex plots thanks to its in-built interface with the R environment.

Mathematical and statistical analyses have been carried out within the R environment (Web sites: R), mostly using the *stats* package from the basic configuration. Curve fitting by *nls* (non-linear least squared) was done either by using the provided models or others described by custom equations. Biochemical simulations were executed by using the *SBMLR* package provided by Bioconductor. It provides an R interface to ordinary differential equation based model solver and is compatible with SBML (Systems Biology Markup Language), a standard language used for the definition of systems biology models based on XML (eXtensible Markup Language), which allows the

sharing of models between different software tools. *Graphics* and *stats* packages from the basic configuration as well as the external package *ggplot2* (Web sites: ggplot2) were used to produce most graphics. The functions provided within the R environment were used either directly, through the RStudio development environment (Web sites: RStudio), or by accessing R through Rserve (Web sites: Rserve) within the MotoCell environment.

Python (Web sites: python) is the programming language used for developing the *PhotoCell* macros operating within the Zen environment by Zeiss used for customised time-lapse image acquisitions and described in *Appendix 10.1*.

3.4. Analysis of cell motility

Diffusive behavior was quantified, within MotoCell, on the basis of mean squared displacement (MSD) and time, by using the "Diffusion" module which fits the function $MSD = kt^{\alpha}$ to data, assigning to each value a weight proportional to the number of averaged squared displacements. Persistence analysis was carried out by using the "Persistence" module, based on formula (3). The mean squared displacements were calculated by collecting and squaring for each path the displacements corresponding to all time intervals between 40 minutes and the full path duration, and then by averaging the squared displacements for each interval.

Time course analyses were performed by separately analyzing overlapping time windows of different length, each spanning a fraction of the total duration of the experiment. Most analyses were automated by writing PHP scripts and executing them within the MotoCell environment.

3.5. Analysis of cell proliferation

Proliferation analyses were curried out within MotoCell by using "Proliferation" module which relies on the *nls* method (available in R) to

determine Weibull parameters through curve fitting on fraction of not-divided cells as function of cell age. The Weibull equation used is reported hereafter:

$$F(x) = \text{Asym} - (\text{Asym} - 1)e^{-e^{\text{lrc}_x \text{shape}}} \quad (14)$$

where *asym* represents the asymptote of the curve; *shape* is a parameter whose value is one if the Weibull reduces to an exponential curve, and becomes bigger as the distribution follows a more sigmoidal curve; *lrc* is a scale parameter that becomes bigger as the curve spreads out.

3.6. Estimating initial protein concentrations

Concentrations of most molecular species introduced in the different developed biochemical models have been taken from quantifications available on literature and were accessed through a database of concentrations representative of different cell types and experimental conditions developed in the laboratory, built by using a standardization method that calculates intracellular protein concentrations starting from data obtained by mass-spectrometry of cell extracts or estimates them from RNAseq.

3.7. Building reactions for developing biochemical model

The biochemical reactions used for developing the ODE based models were modelled by using Michaelis-Menten and mass action laws. Each reaction was written for supporting also inclusion of an extra term introduced to simulate the effect on the reaction of activators and/or inhibitors.

A new sigmoid function was introduced and used to support saturable processes such as transcription by multiple polymerase complexes along a gene:

$$\Delta\text{geneBody.pol} = v \ \text{genePromoter.pol} \ \frac{max - \text{geneBody.pol}}{max} \quad (15)$$

The *max* parameter indicates the maximum capacity of a gene of a given length to support multiple subsequent transcription complexes.

3.8. Generation of simulated cell populations

Simulated datasets used to test the procedure for movement analyses based on the new model were generated by using *SimulCell* (see *Results*). The tool is accessed through a web application used to provide input data, including cell parameters and general features of the experiment, through a dialog box; output data are collected in a text file which records an "experiment" as the result of the simulation of each cell of a given "plate" at each time point. The simulation system mimics the behavior of a cell population by individually simulating each cell as a stochastic entity acting according to defined models representing the main cellular processes, such as growth, proliferation, migration and death. For each simulated moving population, a bias vector and/ or a persistence module are defined, thus producing cell migration patterns ranging between completely diffusive, persistent or biased, in various combinations. No directionally biased and zero persistence movement was obtained by zeroing the corresponding vector.

3.9. Representation of simulated cell morphology

Morphology of synthetic cell populations was represented by using an in-house developed module described elsewhere (in preparation) which supports the generation of cell shapes defined as Bezier curves dependent on cell volume and spreading degree and taking into account movement features.

4. Results

4.1. A three component model for directional cell migration

Although, when observed at relatively low sampling frequency, the movement of cultured eukaryotic cells can effectively be described by a simple diffusion model, at higher sampling rates more complex models, which include additional parameters such as persistence and directionality, are often necessary to obtain a good fit to experimental data. However sometimes difficulties arise as persistence evaluation is not always easy, especially when in presence of a directional bias, as the two parameters tend to interfere with each other with commonly used methods, as detailed below.

4.1.1.Persistence and bias interference in cell movement analysis

To assess the effectiveness of commonly used models, the movement of five different cell lines was followed while grown under standard culture conditions as well as in wound healing experiments, i.e. while recovering from a wound inflicted to the cell layer. This is a condition usually associated with directional motion. The selected cell lines represent a spectrum of mammalian cell types including HeLa, MDA-MB-231 and T24, which are human transformed cell lines isolated from tumours with high metastatic power, NIH-3T3 an established untransformed cell line from murine embryonal fibroblasts and NIH-Ras, a cell line obtained by overexpressing in NIH-3T3 the same constitutively active form of Ras known to be present in T24 cell line. Images of each cell culture were acquired by using *PhotoCell*, a set of macro tools developed to manage time-lapse microscopy acquisitions (see *Appendix*, under 10.1).

Cell movement was characterised by using standard procedures as described under *Material and Methods*: average distance per 40 minute

interval, diffusion parameters (α and k), persistence parameters (s and p) and directional raw bias vector module and angle are reported in Table 2.

cell population		average distance (μm) per 40'	diffusion		persistence		raw bias	
condition	line		k ($\mu m^2/min^\alpha$)	α	s (μm/min)	p (min)	module (μm)	δ (degrees)
random	NIH-3T3	11.3	5.8 ± 2.0	1.14 ± 0.06	0.42 ± 0.06	46 ± 14	0.4	-
	NIH-Ras	14.8	4.6 ± 1.7	1.25 ± 0.04	0.47 ± 0.07	58 ± 20	1.6	
	T24	17.9	4.2 ± 0.7	1.32 ± 0.03	0.52 ± 0.05	65 ± 14	0.8	
	HeLa	6.8	0.4 ± 0.07	1.37 ± 0.03	0.23 ± 0.05	40 ± 19	0.4	
	MDA	5.3	0.2 ± 0.1	1.56 ± 0.09	0.22 ± 0.04	75 ± 36	0.4	
wound	NIH-3T3	9.5	0.1 ± 0.0	1.81 ± 0.05	0.28 ± 0.02	307 ± 85	6.0	13
	NIH-Ras	14.9	0.5 ± 0.1	1.76 ± 0.04	0.40 ± 0.01	479 ± 64	10.8	19
	T24	9.7	0.4 ± 0.1	1.61 ± 0.04	0.33 ± 0.03	134 ± 33	6.0	11
	HeLa	6.6	0.0 ± 0.0	2.00 ± 0.10	0.23 ± 0.05	133 ± 90	4.0	6
	MDA	6.4	0.7 ± 0.1	1.33 ± 0.03	0.24 ± 0.03	55 ± 16	1.2	43
persistent	simulated NIH-3T3	11.8	4.8 ± 0.7	1.18 ± 0.02	0.37 ± 0.01	64 ± 3	1.2	-
biased		11.3	0.1 ± 0.0	1.88 ± 0.01	0.33 ± 0.05	143 ± 55	7.7	1
pers.+ biased		16.8	0.2 ± 0.0	1.94 ± 0.01	0.46 ± 0.04	641 ± 356	14.0	0

Table 2. Superdiffusion of different cell lines in different culture conditions. Five different cells lines (NIH-3T3, NIH-Ras, T24, HeLa and MDA-MB-231) are analysed under standard culture condition (random) and in wound healing experiments (wound) and different motion parameters are calculated: average distance, diffusion (α and k), persistence (s and p) and raw bias (module and δ) parameters. In the last three rows, three simulated NIH-3T3 populations differing for migratory behaviour are analysed and reported.

Average distance was determined by averaging the lengths of all cell displacements observed during each 40 minute interval and varies between 5 and 18 μm according to cell type and experimental conditions. When tested for diffusive motion, all cell lines exhibited a superdiffusive behaviour, with an α coefficient well above 1, which becomes higher, often close to 2, in presence of a wound. The observed superdiffusive movement is typical of most adherent cell lines and it may usually be explained by a combination of directional persistence, related to focal contacts between cell and culture surface (Gail et

al. 1970, ; Hartman et al., 2013; Wang et al., 2001), and a directional bias (raw bias), typical of wound healing experiments. Persistence analysis in Table 2 shows that a degree of persistence (expressed in time units) is always present, with the highest values observed during wound healing. The raw bias, calculated by averaging all cell displacement vectors, has an almost null module in randomly moving populations which becomes much larger after a wound. In wounded populations, the raw bias direction is close to the expected one, as indicated in column δ, reporting the difference between the direction of the raw bias vector and the angle expected from the position of analyzed cells in relation to the wound (0 or 360 degrees for cells located on the left side of a vertically oriented wound, 180 degrees for cells on the right side of it); for randomly moving populations which do not have an expected angle, the δ angle was not calculated. Analysis of bias and persistence parameters in wound healing experiments shows that cell populations with high raw bias also had high persistence, suggesting a possible interference.

To confirm or exclude this hypothesis, three datasets were produced from simulated cell populations corresponding to different experimental situations, where persistence and bias contributions to overall migration were set a priori. For each simulated population, cell paths were generated according to a purely diffusive pattern, modified by adding a fixed amount of persistence and/or directional bias. Under these conditions, the input values used to simulate movement, were assumed to be the expected values when examining the output results. To generate movement patterns in the same range as the experimental ones, the simulation was carried out using an MSD of 100 μm^2, expected to produce an average displacement similar to that observed for NIH-3T3 fibroblasts, while the directional bias was set to 8 μm. Regarding persistence, an 8 μm value was chosen to produce, in directionally unbiased populations, a level of persistence corresponding to about 65 minutes, well

within the range of values observed for the experimental populations. The results are reported in the last three rows of Table 2: cells simulated with no directional bias (p =8 μm and b =0 μm, marked as *persistent* in the Table 2), showed, as expected, a persistence time (p) of 64 minutes and an almost null raw bias vector; for cells following zero persistence motion (p =0 μm and b =8 μm, marked as *biased*), a raw bias vector was detectable as expected, but the obtained persistence time was much higher than the expected null value. For more complex movements, when both bias and persistence were present at the same time (line *pers.+ biased*, p =8 μm and b =8 μm), raw bias module and persistence time were both substantially higher than the expected 8 μm (bias) and 65 minutes (persistence). It appears that by following this approach, bias and persistence cannot always be clearly distinguished and, in the case of combined bias and persistence, both tend to be overestimated.

4.1.2.A new combined model to study movement of cultured cells

To address the previously presented issue, cell motion was modelled as a combination of three vectors: random (r), persistence (p) and bias (b), which, according to cell line and culture conditions, are present in different combinations and contribute to the overall migration (Fig 2). In random movement (Fig 2A), each displacement d consists of an unbiased random vector which can take any possible orientation. In the case of a purely persistent movement (Fig 2B), the displacement d also includes a persistence vector having the direction followed during previous movement (*prev d*). Similarly, a purely biased displacement is modelled as the sum of a random and a bias vector, assumed to be oriented along the bias direction, for example according to a gradient produced by an attractant or another directional stimulus (Fig 2C). In the general case of common experimental conditions, all three vectors are assumed to be present at the same time (Fig 2D): in this case, displacement (d) is the vectorial sum of the persistence (p), bias (b) and

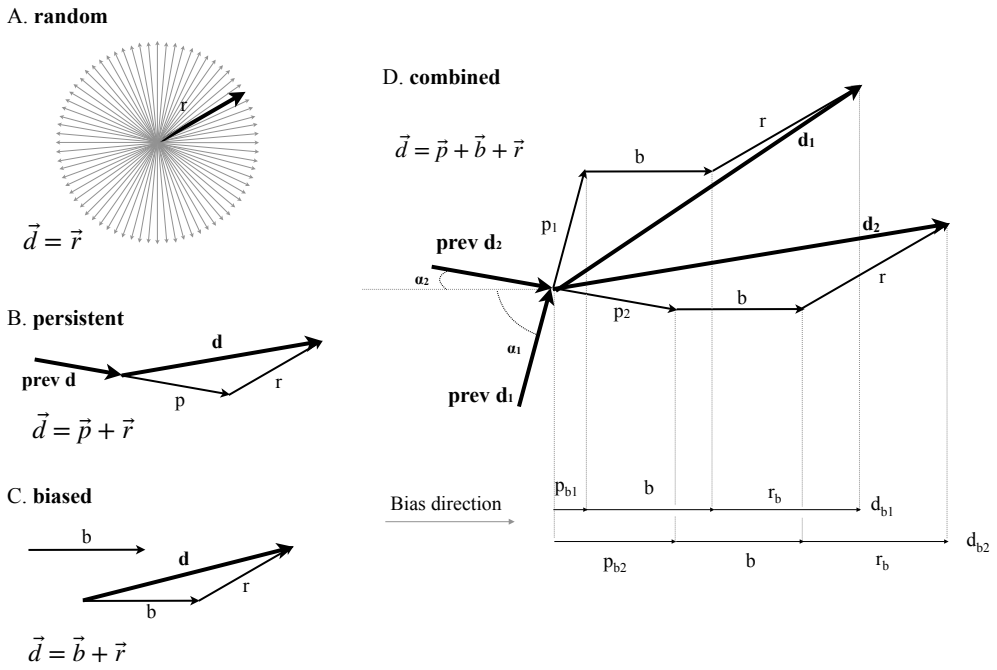

Fig 2. A three component model for single cell movement. In the case of purely diffusive motion (A), cell displacement is modelled as a random vector of radius r. Persistent and biased movement (B and C), respectively add a persistence (p) or bias (b) vector to the random one. In the general case of combined movement (D), displacements are a combination of the three vectors and the directional component (d_b) consists of the whole bias module with the addition of random and persistence contributions (respectively r_b and p_b). The persistence contribution depends on the difference between bias and persistence angle (α angle); its length increases, according to the cosine function, when the α angles decreases.

random (*r*) vectors. Given two different displacements, d_1 and d_2, with the corresponding previous ones (*prev* d_1 and *prev* d_2), and a bias direction, for each of them, the displacement along the bias direction (d_b) is the sum of the whole bias module (*b*) and the random and persistence contributions (r_b and p_b), i.e., the projections of random and persistence vectors onto the bias direction. Random contributions (r_b) to d_b differ among the steps of a path as well as among cells and can be considered as uniformly distributed and tending to zero for large number of displacements. Persistence contribution (p_b) depends instead on the difference between bias and persistence angle (α angle) according to the formula:

$$p_b = p \cdot cos(\alpha) \quad (16)$$

which means that the smaller the α angle, the higher is the contribution of persistence to directionality. In Fig 2D, this relation is graphically explained, where displacements d_1 and d_2, projected on the bias direction, differ for p_{b1} and p_{b2} lengths that depend in turn on α_1 *and* α_2 angles. Thus, the directional component of cell movement as a function of persistence and bias has been defined according to the following function:

$$d_b = b + p \cdot cos(\alpha) \qquad (17)$$

According to the developed model, longer d_b values are obtained for α angles closer to zero, because they include a higher persistence portion. To test whether this relation may be detected in simulated cells, different pairs of p and b parameters were used to produce simulated populations and analysed by plotting, for all displacements, directional component lengths against α angles. Results in Fig 3 show that for random movement, obtained with p=0 μm and b=0 μm (Fig 3A), α angles are homogeneously distributed between -π and +π, while d_b values are symmetrically distributed around zero for all angle values. This is also observed when cell movement is simulated with no bias component, i.e. p=8 μm and b=0 μm (Fig 3B), but in this case d_b values appear to follow a cosine curve, with maximal values for α=0 and minimal ones for α= ± π. When bias is present, with p=0 μm and b=8 μm (Fig 3C), displacement angles are concentrated around the bias direction (α=0) but, for all angles, d_b values are on average offset by a factor corresponding to the bias module. When both bias and persistence are added to the motion, p=8 μm and b=8 μm (Fig 3D), the effects are independently visible as d_b values follow the cosine function and are at the same time offset according to the bias. The previously described formula (17) was used to fit the data in all cases; the curves, reported as continuous lines in each graph, were produced by using the calculated persistence and bias parameters (shown on the top/left for each panel).

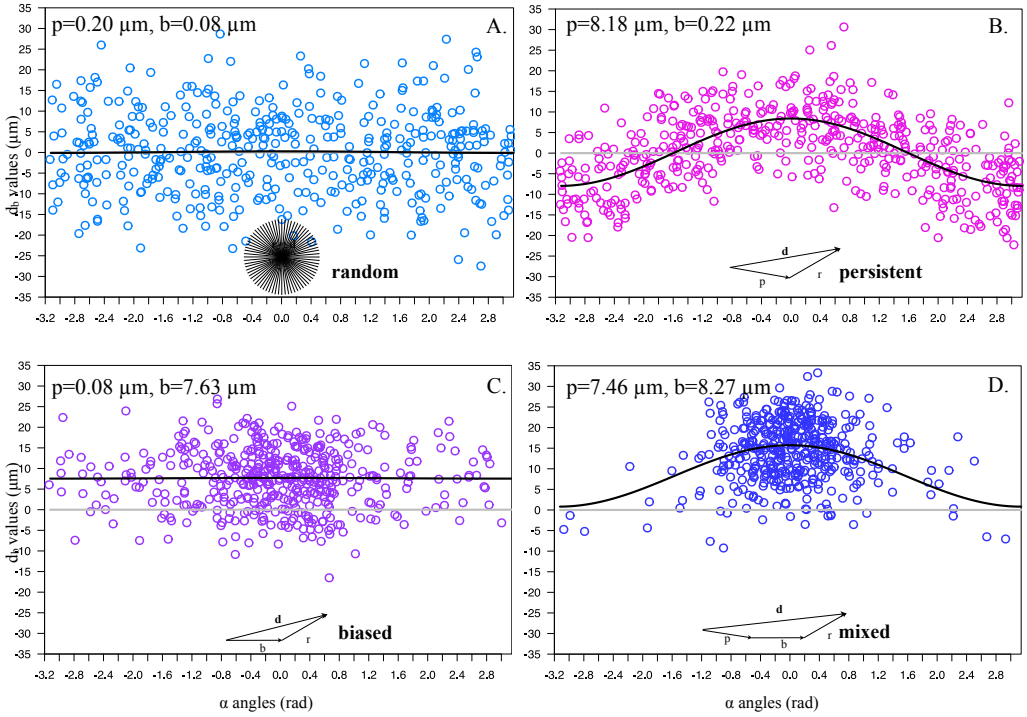

Fig 3. Persistence and bias effect on directional component of cell movement. The directional components of cell displacements from cell populations are plotted (y axis) against their α angles (x axis); (A-D) correspond to populations generated by simulating random (p=0 µm; b=0 µm), persistent (p=8 µm; b=0 µm), biased (p=0 µm; b=8 µm) and mixed movements (p=8 µm; b=8 µm). The continuous line corresponds to curves identified by fitting the described model to the data; the numerical parameters are shown on the top of each graph.

On the basis of these results, the proposed model was considered a good candidate to describe any migratory behaviour and the procedure schematically synthesized in Fig 4, was set up. First, the raw bias vector calculated as the vector sum of all displacement vectors observed in a given time interval is used to obtain the raw bias direction β. After that, for each displacement, the projection onto the raw bias direction (d_b) is determined, as well as the displacement to raw bias angle (α), i.e. the difference between previous displacement and bias direction. The previously defined model (formula 17) is used to fit the directional component lengths (d_b) as a function of α, to obtain bias (b) and persistence (p) modules. Finally, having defined

bias and persistence modules, bias and persistence vectors are subtracted from each displacement, to obtain the random vectors.

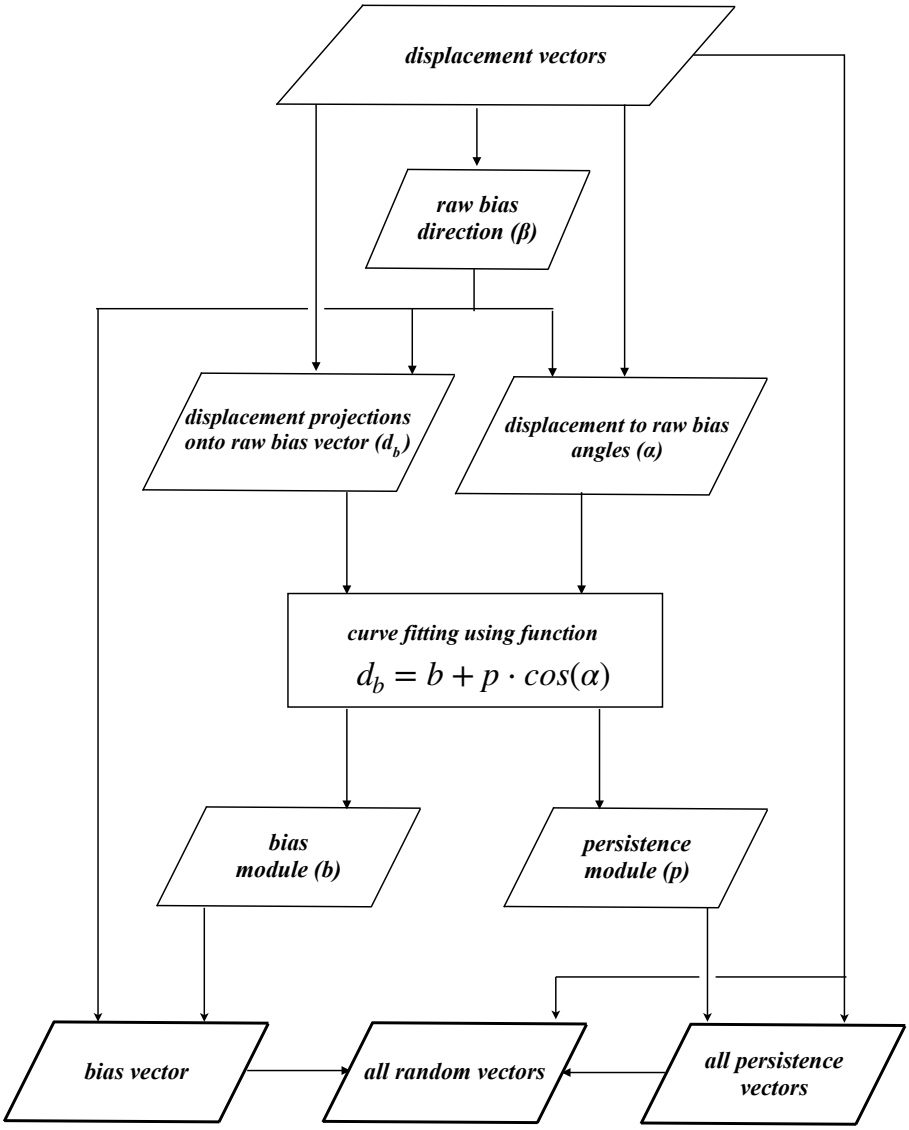

Fig 4. Schematic representation of the procedure for parameters evaluation. It is schematically reported the procedure that, starting from displacement vectors, leads to the calculation of the bias vector, the persistence module and the list of the random vectors deprived of bias and persistence components.

4.1.3.The new model can separately assess persistence and directional bias

The described model and procedure were validated by analyzing cell displacements from datasets obtained from simulated cell populations produced

by using different values of bias, persistence and random module. Each dataset includes the paths followed by 30 cells, generated by using bias and persistence values ranging between 0 and 16 μm, as indicated in the header row and column of Table 3, and a random module equal to 9 μm/40min.

persistence (μm)	bias (μm)											
	0			8			12			16		
	b	*p*	*r*	*b*	*p*	*r*	*b*	*p*	*r*	*b*	*p*	*r*
0	0.4 ± 0.3	-0.4 ± 0.5	8.7	7.8 ± 0.5	-0.2 ± 0.6	8.8	12.3 ± 0.9	-0.2 ± 1.0	8.8	16.6 ± 1.2	-1.1 ± 1.4	8.7
8	0.3 ± 0.3	9.2 ± 0.5	9.1	7.8 ± 0.8	7.9 ± 0.9	9.1	12.0 ± 2.1	8.3 ± 2.3	8.7	13.3 ± 3.8	10.5 ± 4.1	8.8
12	0.0 ± 0.3	12.1 ± 0.5	9.3	6.5 ± 1.4	13.1 ± 1.6	8.9	15.3 ± 4.0	9.4 ± 4.0	8.8	16.7 ± 4.4	11.3 ± 4.6	8.7
16	0.2 ± 0.3	16.2 ± 0.4	8.6	8.2 ± 2.2	15.7 ± 2.4	9.0	11.8 ± 4.3	16.4 ± 4.5	9.0	15.4 ± 7.9	16.3 ± 8.1	9.1

Table 3. Bias, persistence and random estimated from simulated cell populations. The measured bias, persistence and random modules are compared with fixed input bias and persistence (respectively header row and header column) and with random input value (9 μm/40min) used to simulate the synthetic cell movement.

Bias (*b*) and persistence (*p*) values evaluated by the described procedure show that in the case of movement with zero persistence (first row) or no directional bias (first column) calculated bias and persistence modules are very close to the expected values. A similarly good correspondence between expected and measured values was also observed when persistence and bias vectors were both present in combination. The random vectors, calculated for each population, also produced an average module close to the expected value used to generate the simulation.

The same combinations of persistence and bias vectors were also tested for other simulated sets of populations, characterized by different values of random modules, and also in these cases the obtained values show good correspondence with the expected ones, thus proving that the efficacy of the

analysis method is not impaired by changes in the random module (data not shown).

In order to evaluate the performance of the model in relation to cell population size, the previous analysis was repeated using datasets of size ranging between 10 and 100 cells. The results (Fig 5) show that for both bias and persistence values, calculated/expected ratios are within ± 0.4 for datasets of 10 to 20 cells but quickly go down to smaller ones for 30-50 cells and are reduced to within ± 0.1 for bigger datasets (100 cells). This confirms that population sizes used in the evaluations (≥30 cells) are well within the range of acceptability in terms of balance between numerosity of datasets and variability of measured parameters.

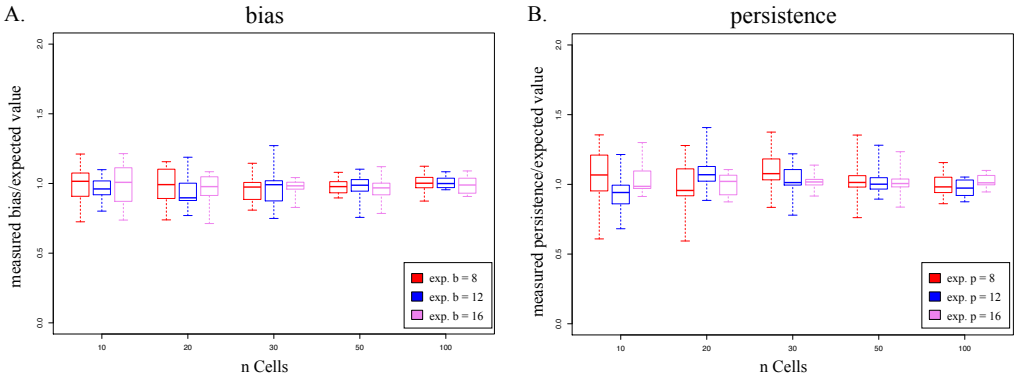

Fig 5. Population size effect on the analysis with the proposed model. For simulated datasets of size ranging between 10 and 100 cells the estimated parameters are reported as ratio between calculated and expected values, the latter are indicated in each graph with distinct colors.

The present model uses, to express persistence, a vector which, combined with a random one, produces the final displacement. Working in this way, persistence depends on random module and may be difficult to evaluate in comparison with other methods which express persistence as a time. In order to facilitate comparison of the two methods, persistence values expressed as time and as vector module were plotted against each other, after normalization, obtained by dividing the persistence time by the time interval (40 minutes in

this case) and persistence vector module by the module of the calculated random vector: the produced values follow a quadratic trend (Fig 6A) which remains the same with simulated datasets of different numerosity and different

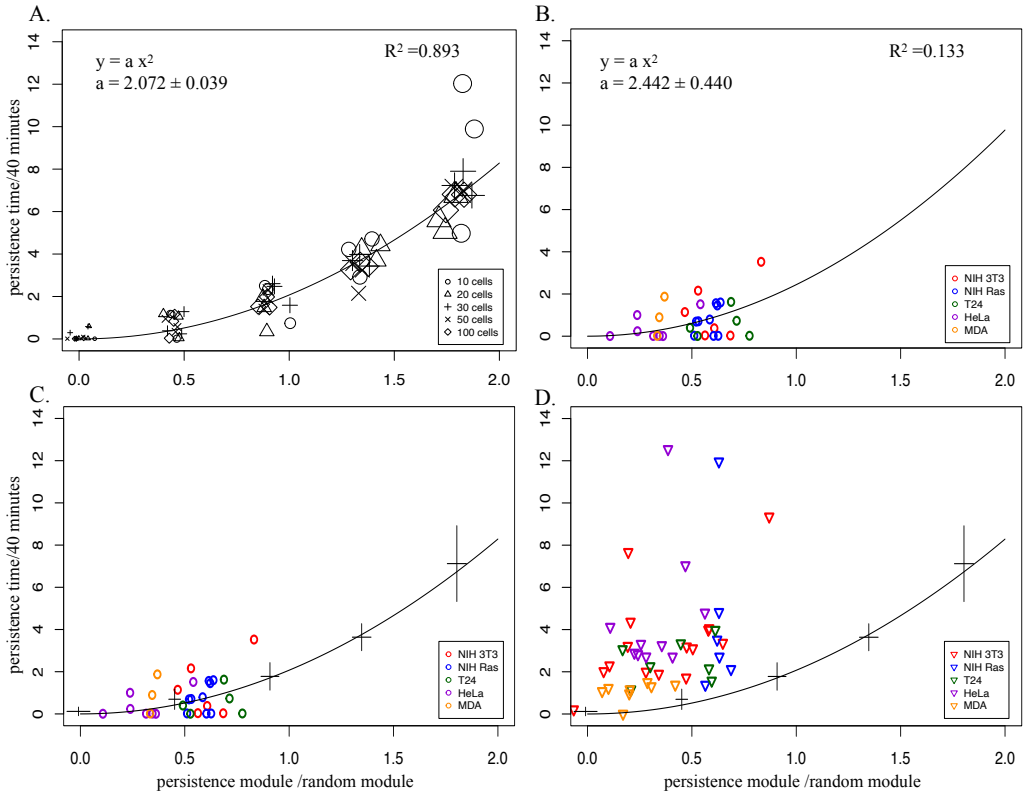

Fig 6. Relation between persistence evaluated as time or as vector length. Persistence values are compared by plotting, for each dataset, the resulting persistence times, normalized against the time interval (40 minutes), versus the persistence module, normalized against the corresponding random module. (A) Persistence values calculated for datasets containing 10 (circle), 20 (triangle), 30 (plus), 50 (cross) or 100 (diamond) cells simulated at different persistence levels (0, 4, 8, 12 and 16 μm) and reported in the plot as symbols of increasing sizes. For each persistence level, three replicated datasets were produced for each cell number. Fitting the indicated quadratic function to the data produced the "a" parameter value and the R^2 determination coefficient reported at the top. The black line represents the curve defined by the calculated "a" parameter. (B) Persistence values calculated as in (A) from NIH-3T3 (red), NIH-Ras (blue), T24 (green), HeLa (violet) and MDA-MB-231 (orange) cells moving in absence of a wound stimulus. The black line corresponds to the curve calculated by fitting the quadratic function to the experimental data as in (A). (C) Persistence values from the (B) plot reported using the same curve as in (A) as a reference; the bars indicate means and standard deviations of the values used to produce the curve. (D) Persistence values calculated for the same cell lines as in (B and C), moving under wound stimulus and plotted using the same reference curve as in (C).

levels of persistence (0, 4, 8, 12, 16 μm). Using a simple quadratic equation for curve fitting, the resulting curve, closely follows the data points, as seen in Fig 6A and confirmed by the determination coefficient R^2, very close to 1. Similar results are shown in Fig 6B, where "time" vs "space" persistence values were calculated from experimental datasets and compared in the same way, after normalization: also in this case the relation produces a quadratic curve which remains very close to the one determined from the simulated data, and characterized by a second power coefficient very close to 2 as before, although with a lower R^2 value. The values reported in Fig 6B, obtained from experimental data with cells moving in absence of directional stimuli, were compared (Fig 6C and 6D) to those obtained from wounded cells, in both cases using, as a reference, curve and standard deviations obtained from the simulated datasets of Fig 6A. While the data points from unstimulated populations are within or close to the range defined by one standard deviation, and represented by using horizontal and vertical traits, the corresponding data points obtained from wounded cells, tend to be located quite far from the quadratic curve, confirming the previous observation that the presence of a directional bias can influence the correct calculation of time persistence.

4.2. Bias and persistence are separate features and play distinct roles in cell movement

The three component model is able to distinguish the role played by each vector in cell movement. The procedure set up to evaluate the three components appears to be effective in independently assessing their values also in "difficult" situations, such as when both bias and persistence are present at the same time. Therefore it was decided to use it on experimental cell populations to better understand the relationship between bias and persistence in cells cultured on plate.

4.2.1.The three component model independently evaluates bias and persistence in experimental cell populations

The experimental datasets initially used in Table 2 were re-analysed with the three component model to separately assess the bias and persistence movement components.

The results are reported, in Table 4, as random, persistence and bias vector modules for a 40 minute time interval; for wound healing experiments, angle δ, i.e. the angle between bias vector and expected migration direction, is also reported. For all cell lines, in absence of wound stimulus, the detected bias has values close to zero and movement, as might be expected, is essentially determined by random and persistence module. Cells with larger average distances show correspondingly higher values for both random and persistence module. For all cell lines, the introduction of a wound stimulus results in a

cell population		average distance (μm) per 40'	random module (μm)	persistence module (μm)	bias	
condition	line				module (μm)	δ (degrees)
random	NIH-3T3	11.3	10.4	4.9 ± 0.6	0.3 ± 0.4	-
	NIH-Ras	14.8	13.2	8.2 ± 0.9	1.1 ± 0.7	
	T24	17.9	15.6	10.7 ± 1.2	1.1 ± 0.9	
	HeLa	6.8	6.7	1.6 ± 0.4	0.5 ± 0.2	
	MDA-MB-231	5.3	5.5	2.0 ± 0.5	0.0 ± 0.3	
wound	NIH-3T3	9.5	7.8	1.5 ± 0.7	5.7 ± 0.6	22.47
	NIH-Ras	14.9	11.1	7.0 ± 2.1	6.1 ± 1.8	19.21
	T24	9.7	7.4	3.3 ± 0.7	4.3 ± 0.6	2.4
	HeLa	6.6	5.9	1.5 ± 0.7	2.9 ± 0.6	5.68
	MDA-MB-231	6.4	6.8	2.8 ± 0.4	1.4 ± 0.3	42.73

Table 4. Characterization of movement of different cell lines in different experimental conditions. The same five experimental cells lines (NIH-3T3, NIH-Ras, T24, HeLa and MDA-MB-231) as in Table 2 are analysed under standard culture condition (random) and in wound healing experiments (wound) and average distance together with the three motion vectors are quantified and reported.

modified movement pattern, affected by a bias vector of higher module than that observed in absence of wound for the same cell lines and oriented along the expected direction, i.e. towards the empty space left by the wound, as indicated by δ angle values ranging between 2 and 43 degrees.

To study movement trends in time and the evolution of its components, the proposed model was also used to analyze HeLa cell populations moving in standard cultures as well as after a wound stimulus. In absence of directional stimulus (Fig 7A-D), all values were essentially stable over time, with movement mainly characterized by random and persistence, while bias remains very low during the whole time. In presence of a wound, higher average distance values were observed (Fig 7E), especially in the time windows immediately following the wound stimulus. At later times, the observed distances tend to be reduced, probably because of the concomitant progressive closure of the wound space, clearly visible in the images acquired at different time points during the experiment (data not shown). The wounded populations showed strong bias, with the highest values at the beginning of the observation time; as time goes by, the bias module tends to be reduced following a trend similar to that observed for the average distance (Fig 7H); the random module does not appear to change accordingly (Fig 7F). Also in this case, the persistence component measured by the new procedure is also not affected by the wound stimulus, even in presence of an increased bias component, and remains within levels close to about half the random module, both in presence (Fig 7G) and in absence (Fig 7C) of wound; it is also not changed when, during the observation time, the wound starts to close.

To comparatively study motion properties of HeLa cells as well as that of other cell lines, data from different populations of HeLa, NIH-3T3, NIH-Ras, T24 and MDA-MB-231 cells were analysed with the presented method.

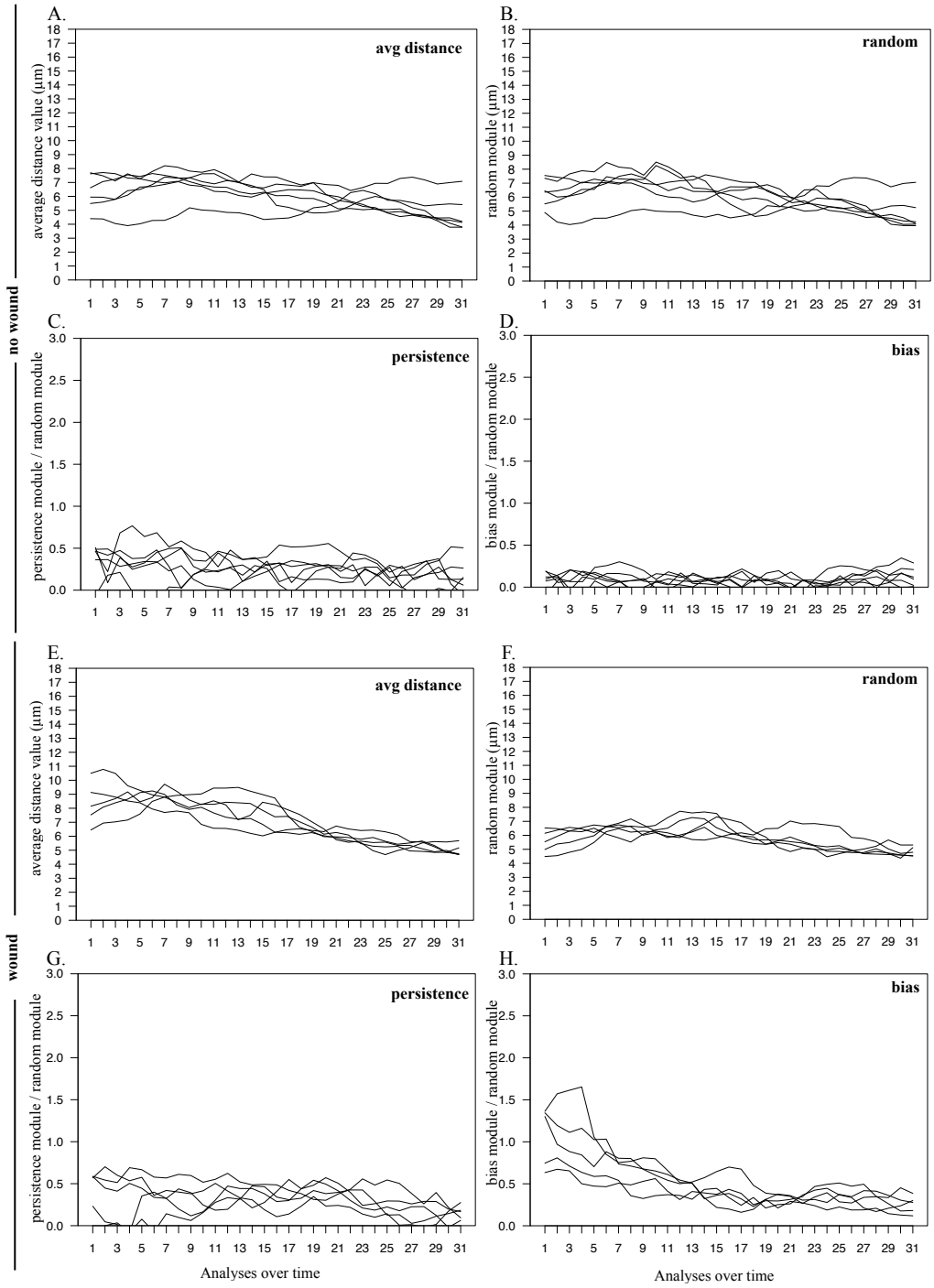

Fig 7. Movement components of HeLa populations over time. HeLa cell movement on a culture plate was evaluated both in absence (A-D) and in presence (E-H) of a wound stimulus. The line plots correspond to independent cell populations; for each of them, the plots report average displacements modules measured over 40 minute steps (A and E), as well as random (B and F) persistence (C and G), and bias (D and H) values, calculated from the observed displacements. Persistence and bias modules were normalized to the corresponding random module. All the values were evaluated at 40 minute intervals using the data from overlapping four hour windows.

In Fig 8, average distance (A) and random component (B) are separately reported for each cell population, as well as persistence (C) and bias (D). Random components vary between different cell lines, being higher for NIH-Ras and T24 cell populations which also show higher average cell displacement modules. All cell lines respond to the wound stimulus with movement characterized by a strong bias component, clearly higher than that observed in its absence; in contrast, persistence is always present with values ranging between 0.4 and 0.8 times the random module and is not significantly modified in presence of a wound stimulus.

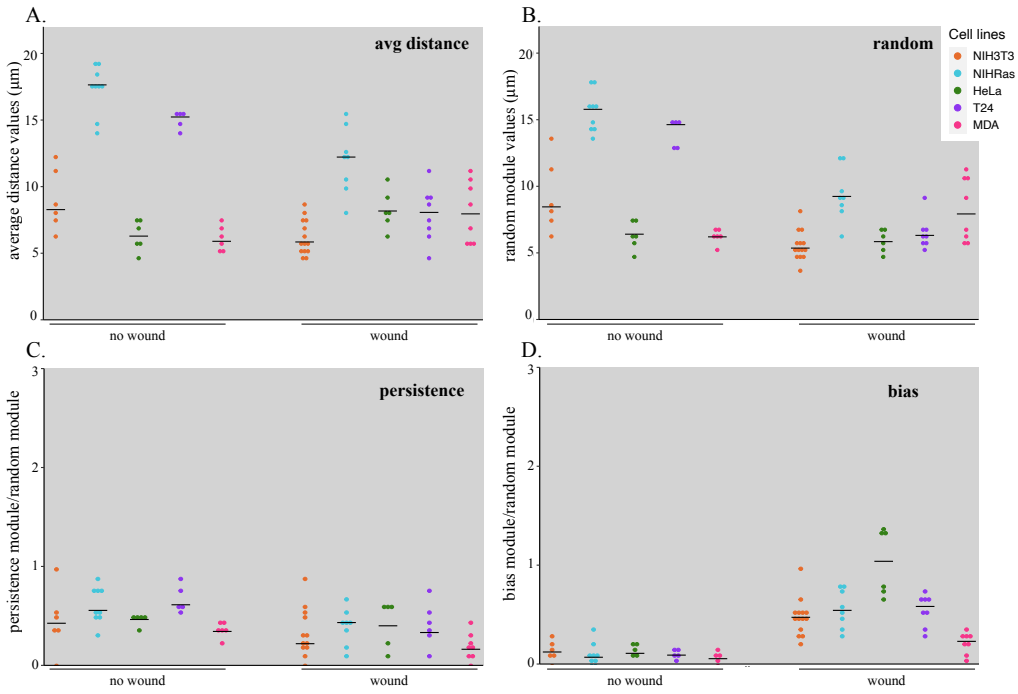

Fig 8. Movement of different cell lines in wound healing experiments. NIH-3T3 (orange), NIH-Ras (blue), HeLa (green), T24 (violet) and MDA-MB-231 (magenta) cell lines were grown on a culture plate and their movement was followed in both standard condition (no wound) and after stimulation (wound) by a wound inflicted to the cell layer. (A) Average distance and (B) random module, (C) persistence and (D) bias. Values reported in (C) and (D) have been normalized against the corresponding random modules. For each cell line, coloured points correspond to independent cultures analysed over a 4 hour time window, while their median value is reported as a small horizontal black trait.

…….

This content will not be available during 2023.

…….

5. Discussion

…….

This content will not be available during 2023.

…….

6. Conclusions

A novel modelling/simulation tool was set up to analyze and simulate cell movement. Crucial to this end was a new model describing movement in terms of three components, random motion, persistence and directional bias, which differently affect cell movement and may be independently controlled by different drugs. The model allowed to quantitatively analyse experimental cell populations and was used for stochastic simulation of cell movement, to generate synthetic cell populations within *SimulCell*, an *in silico* simulation tool developed in the laboratory. Synthetic cell populations produced in this way rely on stochastic models and are controlled by molecular simulation of the cell cycle and pathways signalling the presence of extracellular factors. To produce hour-long simulations, where proteins are degraded and synthesized in time, a dedicated ODE based module was set up to simulate *de novo* protein synthesis by gene transcription and mRNA translation. Following this approach, simulated cells grow and split according to a molecular model of cell cycle progression, driven by linking replication to cell mass and volumetric growth and regulated by a biochemical model of the EGFR/ERK pathway. In its present state, the developed system opens up new options for studying proliferation and movement and improving the comprehension of their regulation.

7. Acknowledgements

At this point, I would like to thank special people who helped and supported me in improving my training, studies and results.

My first acknowledgements are to Professor Giovanni Paolella, who has taught me all what I am able to do today. Thanks for giving me your trust and endurance since I was a bachelor student. Thanks for teaching to not settle for sufficiently good results and for stimulating me in going deeper and beyond in improving my understanding, methods and results. Thanks for your support, for your brilliant suggestions and explanations, for giving me the opportunity and stimuli for learning every day new topics and techniques. Thanks understanding my ideas and opinions and for seconding my attitudes and interests.

I wish to thank Leandra Sepe for having supported me in every moment and situation during these seven years. Thanks for teaching me the many techniques for culturing cells and observing them at the microscope. Thanks for our complicity and for having been a point of reference many times.

Thanks to Angelo Boccia for his openness towards helping me all the days of the week. Thanks for having been patient with me when I was not jet expert and I had to learn new techniques and approaches for our genomic experiments and studies.

I would like to mention Elena Cimmino and Davide Scognamiglio with whom we managed to create a very cohesive lab team where we could reciprocally help and support with no space for useless competitions and jealousies. Thanks for all the times you trusted my word and suggestions because this helped me to learn how to deal with younger researchers and, at the same time, to have more faith in me and my ideas. And thanks for your continuous support and our “anti-stress” walks and aperitifs.

My last special thanks are for my parents, for their constant support and trust in my choices and dreams. Thanks my little sister Giusy who supported and encouraging me everyday; thanks for being an example of strength and courage. Thanks my grandfather who have never left me alone and have made me able to face also the more difficult situations.

8. List of Publications

The following publications include in full or in part results obtained during the preparation of the present thesis:

Toscano E, Sepe L, Del Giudice G, Tufano R, Paolella G. A three component model for superdiffusive motion effectively describes migration of eukaryotic cells moving freely or under a directional stimulus. PLoS One. 2022 Aug 2;17(8):e0272259. doi: 10.1371/journal.pone.0272259. PMID: 35917375; PMCID: PMC9345344.

Toscano E, del Giudice G, Cimmino E, Sepe L, Paolella G. *SimulCell*: an *in silico* simulation tool which accurately reproduces the behaviour of migrating cell populations. (Manuscript in preparation)

Toscano E, Cimmino E, Caggiano R, Boccia A, Sepe L, Paolella G. Controlling *in silico* simulation of growth and cell cycle progression of synthetic cell populations within *SimulCell* by ODE based molecular models. (Manuscript in preparation)

9. References

1. Aguda BD, Tang Y. The kinetic origins of the restriction point in the mammalian cell cycle. Cell Prolif. 1999;32(5):321-335. doi:10.1046/j.1365-2184.1999.3250321.x
2. Alfieri R, Barberis M, Chiaradonna F, et al. Towards a systems biology approach to mammalian cell cycle: modeling the entrance into S phase of quiescent fibroblasts after serum stimulation. BMC Bioinformatics. 2009;10 Suppl 12(Suppl 12):S16. Published 2009 Oct 15. doi:10.1186/1471-2105-10-S12-S16
3. Alt, W. and G. Hoffmann (1990). "Correlation analysis of two-dimensional locomotion paths." Biological Motion 89:254.
4. Amati B, Vlach J. Kip1 meets SKP2: new links in cell-cycle control. Nat Cell Biol. 1999;1(4):E91-E93. doi:10.1038/12087
5. Anand-Apte B, Zetter BR, Viswanathan A, et al. Platelet-derived growth factor and fibronectin-stimulated migration are differentially regulated by the Rac and extracellular signal-regulated kinase pathways. J Biol Chem. 1997;272(49):30688-30692. doi:10.1074/jbc.272.49.30688
6. Ardehali MB, Lis JT. Tracking rates of transcription and splicing in vivo. Nat Struct Mol Biol. 2009;16(11):1123-1124. doi:10.1038/nsmb1109-1123
7. Barberis M, Klipp E, Vanoni M, Alberghina L. Cell size at S phase initiation: an emergent property of the G1/S network. PLoS Comput Biol. 2007;3(4):e64. doi:10.1371/journal.pcbi.0030064
8. Barh D, Yiannakopoulou EC, Salawu EO, et al. In silico disease model: from simple networks to complex diseases. *Animal Biotechnology*. 2020;441-460. doi:10.1016/B978-0-12-811710-1.00020-3
9. Bartek J, Bartkova J, Lukas J. The retinoblastoma protein pathway and the restriction point. Curr Opin Cell Biol. 1996;8(6):805-814. doi:10.1016/s0955-0674(96)80081-0
10. Bentley, J. G. W.. “Modelling circular data using a mixture of von mises and uniform distribution.” (2006).
11. Biggin MD. Animal transcription networks as highly connected, quantitative continua. Dev Cell. 2011;21(4):611-626. doi:10.1016/j.devcel.2011.09.008
12. Bindschadler M, McGrath JL. Sheet migration by wounded monolayers as an emergent property of single-cell dynamics. J Cell Sci. 2007;120(Pt 5):876-884. doi:10.1242/jcs.03395

13. Boucrot E, Kirchhausen T. Endosomal recycling controls plasma membrane area during mitosis. Proc Natl Acad Sci U S A. 2007;104(19):7939-7944. doi:10.1073/pnas.0702511104

14. Brocchieri L, Karlin S. Protein length in eukaryotic and prokaryotic proteomes. Nucleic Acids Res. 2005;33(10):3390-3400. Published 2005 Jun 10. doi:10.1093/nar/gki615

15. Bubeník J, Baresová M, Viklický V, Jakoubková J, Sainerová H, Donner J. Established cell line of urinary bladder carcinoma (T24) containing tumour-specific antigen. Int J Cancer. 1973;11(3):765-773. doi:10.1002/ijc.2910110327

16. Buck SB, Bradford J, Gee KR, Agnew BJ, Clarke ST, Salic A. Detection of S-phase cell cycle progression using 5-ethynyl-2'-deoxyuridine incorporation with click chemistry, an alternative to using 5-bromo-2'-deoxyuridine antibodies. Biotechniques. 2008;44(7):927-929. doi:10.2144/000112812

17. Cadart C, Zlotek-Zlotkiewicz E, Venkova L, et al. Fluorescence eXclusion Measurement of volume in live cells. Methods Cell Biol. 2017;139:103-120. doi:10.1016/bs.mcb.2016.11.009

18. Cadart C, Monnier S, Grilli J, et al. Size control in mammalian cells involves modulation of both growth rate and cell cycle duration. Nat Commun. 2018;9(1):3275. Published 2018 Aug 16. doi:10.1038/s41467-018-05393-0

19. Cadart, C., Venkova, L., Recho, P. et al. The physics of cell-size regulation across timescales. Nat. Phys. 15, 993–1004 (2019). https://doi.org/10.1038/s41567-019-0629-y

20. Cadart C, Venkova L, Piel M, Cosentino Lagomarsino M. Volume growth in animal cells is cell cycle dependent and shows additive fluctuations. Elife. 2022;11:e70816. Published 2022 Jan 28. doi:10.7554/eLife.70816

21. Cailleau R, Young R, Olivé M, Reeves WJ Jr. Breast tumor cell lines from pleural effusions. J Natl Cancer Inst. 1974;53(3):661-674. doi:10.1093/jnci/53.3.661

22. Campos M, Surovtsev IV, Kato S, et al. A constant size extension drives bacterial cell size homeostasis. Cell. 2014;159(6):1433-1446. doi:10.1016/j.cell.2014.11.022

23. Cantarella C, Sepe L, Fioretti F, Ferrari MC, Paolella G. Analysis and modelling of motility of cell populations with MotoCell. BMC Bioinformatics. 2009;10 Suppl 12(Suppl 12):S12. Published 2009 Oct 15. doi:10.1186/1471-2105-10-S12-S12

24. Cappell SD, Mark KG, Garbett D, Pack LR, Rape M, Meyer T. EMI1 switches from being a substrate to an inhibitor of APC/CCDH1 to start the cell cycle. Nature. 2018;558(7709):313-317. doi:10.1038/s41586-018-0199-7

25. Castellone RD, Leffler NR, Dong L, Yang LV. Inhibition of tumor cell migration and metastasis by the proton-sensing GPR4 receptor. Cancer Lett. 2011;312(2):197-208. doi:10.1016/j.canlet.2011.08.013

26. Castro A, Bernis C, Vigneron S, Labbé JC, Lorca T. The anaphase-promoting complex: a key factor in the regulation of cell cycle. Oncogene. 2005;24(3):314-325. doi:10.1038/sj.onc.1207973

27. Chapnick DA, Jacobsen J, Liu X. The development of a novel high throughput computational tool for studying individual and collective cellular migration. PLoS One. 2013;8(12):e82444. Published 2013 Dec 27. doi:10.1371/journal.pone.0082444

28. Chen KC, Csikasz-Nagy A, Gyorffy B, Val J, Novak B, Tyson JJ. Kinetic analysis of a molecular model of the budding yeast cell cycle. Mol Biol Cell. 2000;11(1):369-391. doi:10.1091/mbc.11.1.369

29. Chen H, Zhu G, Li Y, et al. Extracellular signal-regulated kinase signaling pathway regulates breast cancer cell migration by maintaining slug expression. Cancer Res. 2009;69(24):9228-9235. doi:10.1158/0008-5472.CAN-09-1950

30. Cho P, Schneider GB, Kellogg B, Zaharias R, Keller JC. Effect of glucocorticoid-induced osteoporotic-like conditions on osteoblast cell attachment to implant surface microtopographies. Implant Dent. 2006;15(4):377-385. doi:10.1097/01.id.0000247858.37697.d5

31. Codling EA, Plank MJ, Benhamou S. Random walk models in biology. J R Soc Interface. 2008;5(25):813-834. doi:10.1098/rsif.2008.0014

32. Coller HA, Sang L, Roberts JM. A new description of cellular quiescence. PLoS Biol. 2006;4(3):e83. doi:10.1371/journal.pbio.0040083

33. Collins JM. Rates of DNA synthesis during the S-phase of HeLa cells. J Biol Chem. 1978;253(23):8570-8577.

34. Cooper S. Control and maintenance of mammalian cell size. BMC Cell Biol. 2004;5(1):35. Published 2004 Sep 29. doi:10.1186/1471-2121-5-35

35. Cooray P, Yuan Y, Schoenwaelder SM, Mitchell CA, Salem HH, Jackson SP. Focal adhesion kinase (pp125FAK) cleavage and regulation by calpain. Biochem J. 1996;318 (Pt 1)(Pt 1):41-47. doi:10.1042/bj3180041

36. Cordelières FP, Petit V, Kumasaka M, et al. Automated cell tracking and analysis in phase-contrast videos (iTrack4U): development of Java software based on combined mean-shift processes. PLoS One. 2013;8(11):e81266. Published 2013 Nov 27. doi:10.1371/journal.pone.0081266

37. Cross FR, Roberts JM. Retinoblastoma protein: combating algal bloom. Curr Biol. 2001;11(20):R824-R827. doi:10.1016/s0960-9822(01)00495-x

38. Csikász-Nagy A, Battogtokh D, Chen KC, Novák B, Tyson JJ. Analysis of a generic model of eukaryotic cell-cycle regulation. Biophys J. 2006;90(12):4361-4379. doi:10.1529/biophysj.106.081240

39. Darzynkiewicz Z, Traganos F, Zhao H, Halicka HD, Li J. Cytometry of DNA replication and RNA synthesis: Historical perspective and recent advances based on "click chemistry". Cytometry A. 2011;79(5):328-337. doi:10.1002/cyto.a.21048

40. Dasika GK, Lin SC, Zhao S, Sung P, Tomkinson A, Lee EY. DNA damage-induced cell cycle checkpoints and DNA strand break repair in development and tumorigenesis. Oncogene. 1999;18(55):7883-7899. doi:10.1038/sj.onc.1203283

41. Davey NE, Morgan DO. Building a Regulatory Network with Short Linear Sequence Motifs: Lessons from the Degrons of the Anaphase-Promoting Complex. Mol Cell. 2016;64(1):12-23. doi:10.1016/j.molcel.2016.09.006

42. David-Pfeuty T. The flexible evolutionary anchorage-dependent Pardee's restriction point of mammalian cells: how its deregulation may lead to cancer. Biochim Biophys Acta. 2006;1765(1):38-66. doi:10.1016/j.bbcan.2005.08.008

43. de Boer, H Rudolf et al. “Controlling the response to DNA damage by the APC/C-Cdh1.” *Cellular and molecular life sciences : CMLS* vol. 73,5 (2016): 949-60. doi:10.1007/s00018-015-2096-7

44. Debeir O, Van Ham P, Kiss R, Decaestecker C. Tracking of migrating cells under phase-contrast video microscopy with combined mean-shift processes. IEEE Trans Med Imaging. 2005;24(6):697-711. doi:10.1109/TMI.2005.846851

45. Deforet M, Parrini MC, Petitjean L, et al. Automated velocity mapping of migrating cell populations (AVeMap). Nat Methods. 2012;9(11):1081-1083. doi:10.1038/nmeth.2209

46. Deforet M, van Ditmarsch D, Xavier JB. Cell-Size Homeostasis and the Incremental Rule in a Bacterial Pathogen. Biophys J. 2015;109(3):521-528. doi:10.1016/j.bpj.2015.07.002

47. DeGregori J. The genetics of the E2F family of transcription factors: shared functions and unique roles. Biochim Biophys Acta. 2002;1602(2):131-150. doi:10.1016/s0304-419x(02)00051-3

48. Deplanche M, Filho RA, Alekseeva L, et al. Phenol-soluble modulin α induces G2/M phase transition delay in eukaryotic HeLa cells. FASEB J. 2015;29(5):1950-1959. doi:10.1096/fj.14-260513

49. Dickinson, R.B. and R.T. Tranquillo (1993). "Optimal estimation of cell movement indices from the statistical analysis of cell tracking data." AIChE J 39(12): 1995-2010.

50. PA DiMilla, JA Stone, JA Quinn, SM Albelda, DA Lauffenburger; Maximal migration of human smooth muscle cells on fibronectin and type IV collagen occurs at an intermediate attachment strength. J Cell Biol 1 August 1993; 122 (3): 729–737. doi: https://doi.org/10.1083/jcb.122.3.729

51. Dohadwala M, da Cruz e Silva EF, Hall FL, et al. Phosphorylation and inactivation of protein phosphatase 1 by cyclin-dependent kinases. Proc Natl Acad Sci U S A. 1994;91(14):6408-6412. doi:10.1073/pnas.91.14.6408

52. Dolbeare F, Gratzner H, Pallavicini MG, Gray JW. Flow cytometric measurement of total DNA content and incorporated bromodeoxyuridine. Proc Natl Acad Sci U S A. 1983;80(18):5573-5577. doi:10.1073/pnas.80.18.5573

53. Dolznig H, Grebien F, Sauer T, Beug H, Müllner EW. Evidence for a size-sensing mechanism in animal cells. Nat Cell Biol. 2004;6(9):899-905. doi:10.1038/ncb1166

54. Dunn GA, Brown AF. A unified approach to analysing cell motility. J Cell Sci Suppl. 1987;8:81-102. doi:10.1242/jcs.1987.supplement_8.5

55. Fantes PA. Control of cell size and cycle time in Schizosaccharomyces pombe. J Cell Sci. 1977;24:51-67. doi:10.1242/jcs.24.1.51

56. Fenteany G, Janmey PA, Stossel TP. Signaling pathways and cell mechanics involved in wound closure by epithelial cell sheets. Curr Biol. 2000;10(14):831-838. doi:10.1016/s0960-9822(00)00579-0

57. Fincham VJ, James M, Frame MC, Winder SJ. Active ERK/MAP kinase is targeted to newly forming cell-matrix adhesions by integrin engagement and v-Src. EMBO J. 2000;19(12):2911-2923. doi:10.1093/emboj/19.12.2911

58. Finka A, Goloubinoff P. Proteomic data from human cell cultures refine mechanisms of chaperone-mediated protein homeostasis. Cell Stress Chaperones. 2013;18(5):591-605. doi:10.1007/s12192-013-0413-3

59. Flomerfelt FA, Gress RE. Analysis of Cell Proliferation and Homeostasis Using EdU Labeling. Methods Mol Biol. 2016;1323:211-220. doi:10.1007/978-1-4939-2809-5_18

60. Forester CM, Maddox J, Louis JV, Goris J, Virshup DM. Control of mitotic exit by PP2A regulation of Cdc25C and Cdk1. Proc Natl Acad Sci U S A. 2007;104(50):19867-19872. doi:10.1073/pnas.0709879104

61. Fuchs G, Voichek Y, Benjamin S, Gilad S, Amit I, Oren M. 4sUDRB-seq: measuring genomewide transcriptional elongation rates and initiation frequencies within cells. Genome Biol. 2014;15(5):R69. Published 2014 May 9. doi:10.1186/gb-2014-15-5-r69

62. Fürth, R. Die Brownsche Bewegung bei Berücksichtigung einer Persistenz der Bewegungsrichtung. Mit Anwendungen auf die Bewegung lebender Infusorien. Z. Physik 2, 244–256 (1920). https://doi.org/10.1007/BF01328731

63. Gail MH, Boone CW. The locomotion of mouse fibroblasts in tissue culture. Biophys J. 1970;10(10):980-993. doi:10.1016/S0006-3495(70)86347-0

64. Gallenberger M, zu Castell W, Hense BA, Kuttler C. Dynamics of glucose and insulin concentration connected to the β-cell cycle: model development and analysis. Theor Biol Med Model. 2012;9:46. Published 2012 Nov 19. doi:10.1186/1742-4682-9-46

65. Gauthier NC, Rossier OM, Mathur A, Hone JC, Sheetz MP. Plasma membrane area increases with spread area by exocytosis of a GPI-anchored protein compartment. Mol Biol Cell. 2009;20(14):3261-3272. doi:10.1091/mbc.e09-01-0071

66. Gebäck T, Schulz MM, Koumoutsakos P, Detmar M. TScratch: a novel and simple software tool for automated analysis of monolayer wound healing assays. Biotechniques. 2009;46(4):265-274. doi:10.2144/000113083

67. Geiger B, Spatz JP, Bershadsky AD. Environmental sensing through focal adhesions. Nat Rev Mol Cell Biol. 2009;10(1):21-33. doi:10.1038/nrm2593

68. Gérard C, Tyson JJ, Novák B. Minimal models for cell-cycle control based on competitive inhibition and multisite phosphorylations of Cdk substrates. Biophys J. 2013;104(6):1367-1379. doi:10.1016/j.bpj.2013.02.012

69. Gey GO, Coffman WD, Kubicek MT. Tissue culture studies of the proliferative capacity of cervical carcinoma and normal epithelium. Cancer Res. 1952;

70. Gheghiani L, Loew D, Lombard B, Mansfeld J, Gavet O. PLK1 Activation in Late G2 Sets Up Commitment to Mitosis. Cell Rep. 2017;19(10):2060-2073. doi:10.1016/j.celrep.2017.05.031

71. Ginzberg MB, Chang N, D'Souza H, Patel N, Kafri R, Kirschner MW. Cell size sensing in animal cells coordinates anabolic growth rates and cell cycle progression to maintain cell size uniformity. Elife. 2018;7:e26957. Published 2018 Jun 11. doi:10.7554/eLife.26957

72. Glading A, Bodnar RJ, Reynolds IJ, et al. Epidermal growth factor activates m-calpain (calpain II), at least in part, by extracellular signal-regulated kinase-mediated phosphorylation. Mol Cell Biol. 2004;24(6):2499-2512. doi:10.1128/MCB.24.6.2499-2512.2004

73. Goldbeter A. A minimal cascade model for the mitotic oscillator involving cyclin and cdc2 kinase. Proc Natl Acad Sci U S A. 1991;88(20):9107-9111. doi:10.1073/pnas.88.20.9107

74. Gompertz, Benjamin. “On the Nature of the Function Expressive of the Law of Human Mortality, and on a New Mode of Determining the Value of Life Contingencies.” Philosophical Transactions of the Royal Society of London 115 (1825): 513–83. http://www.jstor.org/stable/107756.

75. Gorelik R, Gautreau A. Quantitative and unbiased analysis of directional persistence in cell migration. Nat Protoc. 2014;9(8):1931-1943. doi:10.1038/nprot.2014.131

76. Haberichter T, Mädge B, Christopher RA, Yoshioka N, Dhiman A, Miller R, Gendelman R, Aksenov SV, Khalil IG, Dowdy SF. A systems biology dynamical model of mammalian G1 cell cycle progression. Mol Syst Biol. 2007;3:84. doi: 10.1038/msb4100126. Epub 2007 Feb 13. PMID: 17299420; PMCID: PMC1828753.

77. Hall A. The cytoskeleton and cancer. Cancer Metastasis Rev. 2009;28(1-2):5-14. doi:10.1007/s10555-008-9166-3

78. Hartman ZR, Schaller MD, Agazie YM. The tyrosine phosphatase SHP2 regulates focal adhesion kinase to promote EGF-induced lamellipodia persistence and cell migration. Mol Cancer Res. 2013;11(6):651-664. doi:10.1158/1541-7786.MCR-12-0578

79. Heit B, Tavener S, Raharjo E, Kubes P. An intracellular signaling hierarchy determines direction of migration in opposing chemotactic gradients. J Cell Biol. 2002;159(1):91-102. doi:10.1083/jcb.200202114

80. Herrick J, Jun S, Bechhoefer J, Bensimon A. Kinetic model of DNA replication in eukaryotic organisms. J Mol Biol. 2002;320(4):741-750. doi:10.1016/s0022-2836(02)00522-3

81. Hirohashi S, Kanai Y. Cell adhesion system and human cancer morphogenesis. Cancer Sci. 2003;94(7):575-581. doi:10.1111/j.1349-7006.2003.tb01485.x

82. Hong J, Zhou J, Fu J, et al. Phosphorylation of serine 68 of Twist1 by MAPKs stabilizes Twist1 protein and promotes breast cancer cell invasiveness. Cancer Res. 2011;71(11):3980-3990. doi:10.1158/0008-5472.CAN-10-2914

83. Huang S, Ingber DE. The structural and mechanical complexity of cell-growth control. *Nat Cell Biol*. 1999;1(5):E131-E138. doi:10.1038/13043

84. Huang C, Jacobson K, Schaller MD. MAP kinases and cell migration. J Cell Sci. 2004;117(Pt 20):4619-4628. doi:10.1242/jcs.01481

85. Huttenlocher A, Ginsberg MH, Horwitz AF. Modulation of cell migration by integrin-mediated cytoskeletal linkages and ligand-binding affinity. J Cell Biol. 1996;134(6):1551-1562. doi:10.1083/jcb.134.6.1551

86. Huttenlocher A, Palecek SP, Lu Q, et al. Regulation of cell migration by the calcium-dependent protease calpain. J Biol Chem. 1997;272(52):32719-32722. doi:10.1074/jbc.272.52.32719

87. Ichikawa K, Kubota Y, Nakamura T, et al. MCRIP1, an ERK substrate, mediates ERK-induced gene silencing during epithelial-mesenchymal transition by regulating the co-repressor CtBP. Mol Cell. 2015;58(1):35-46. doi:10.1016/j.molcel.2015.01.023

88. Ingolia NT, Lareau LF, Weissman JS. Ribosome profiling of mouse embryonic stem cells reveals the complexity and dynamics of mammalian proteomes. Cell. 2011;147(4):789-802. doi:10.1016/j.cell.2011.10.002

89. Iwamoto K, Tashima Y, Hamada H, Eguchi Y, Okamoto M. Mathematical modeling and sensitivity analysis of G1/S phase in the cell cycle including the DNA-damage signal transduction pathway. Biosystems. 2008;94(1-2):109-117. doi:10.1016/j.biosystems.2008.05.016

90. Iyer VR, Eisen MB, Ross DT, et al. The transcriptional program in the response of human fibroblasts to serum. Science. 1999;283(5398):83-87. doi:10.1126/science.283.5398.83

91. Jung Y, Kraikivski P, Shafiekhani S, Terhune SS, Dash RK. Crosstalk between Plk1, p53, cell cycle, and G2/M DNA damage checkpoint regulation in cancer: computational modeling and analysis. NPJ Syst Biol Appl. 2021;7(1):46. Published 2021 Dec 9. doi:10.1038/s41540-021-00203-8

92. Kafri R, Levy J, Ginzberg MB, Oh S, Lahav G, Kirschner MW. Dynamics extracted from fixed cells reveal feedback linking cell growth to cell cycle. Nature. 2013;494(7438):480-483. doi:10.1038/nature11897

93. Keenan TM, Folch A. Biomolecular gradients in cell culture systems. Lab Chip. 2008;8(1):34-57. doi:10.1039/b711887b

94. Kelly T, Callegari AJ. Dynamics of DNA replication in a eukaryotic cell. Proc Natl Acad Sci U S A. 2019;116(11):4973-4982. doi:10.1073/pnas.1818680116

95. Khalili AA, Ahmad MR. A Review of Cell Adhesion Studies for Biomedical and Biological Applications. Int J Mol Sci. 2015;16(8):18149-18184. Published 2015 Aug 5. doi:10.3390/ijms160818149

96. Kim BJ, Wu M. Microfluidics for mammalian cell chemotaxis. Ann Biomed Eng. 2012;40(6):1316-1327. doi:10.1007/s10439-011-0489-9

97. Kimura H, Tao Y, Roeder RG, Cook PR. Quantitation of RNA polymerase II and its transcription factors in an HeLa cell: little soluble holoenzyme but significant amounts of polymerases attached to the nuclear substructure. Mol Cell Biol. 1999;19(8):5383-5392. doi:10.1128/MCB.19.8.5383

98. Klemke RL, Cai S, Giannini AL, Gallagher PJ, de Lanerolle P, Cheresh DA. Regulation of cell motility by mitogen-activated protein kinase. J Cell Biol. 1997;137(2):481-492. doi:10.1083/jcb.137.2.481

99. Kohn KW. Functional capabilities of molecular network components controlling the mammalian G1/S cell cycle phase transition. Oncogene. 1998;16(8):1065-1075. doi:10.1038/sj.onc.1201608

100.Krueger JS, Keshamouni VG, Atanaskova N, Reddy KB. Temporal and quantitative regulation of mitogen-activated protein kinase (MAPK) modulates cell motility and invasion. Oncogene. 2001;20(31):4209-4218. doi:10.1038/sj.onc.1204541

101.Kühn S, Geyer M. Formins as effector proteins of Rho GTPases. Small GTPases. 2014;5:e29513. doi:10.4161/sgtp.29513

102.Kwon YG, Lee SY, Choi Y, Greengard P, Nairn AC. Cell cycle-dependent phosphorylation of mammalian protein phosphatase 1 by cdc2 kinase. Proc Natl Acad Sci U S A. 1997;94(6):2168-2173. doi:10.1073/pnas.94.6.2168

103.Lev Bar-Or R, Maya R, Segel LA, Alon U, Levine AJ, Oren M. Generation of oscillations by the p53-Mdm2 feedback loop: a theoretical and experimental study. Proc Natl Acad Sci U S A. 2000;97(21):11250-11255. doi:10.1073/pnas.210171597

104.Li JJ, Bickel PJ, Biggin MD. System wide analyses have underestimated protein abundances and the importance of transcription in mammals. PeerJ. 2014;2:e270. Published 2014 Feb 27. doi:10.7717/peerj.270

105.Lindqvist A, Rodríguez-Bravo V, Medema RH. The decision to enter mitosis: feedback and redundancy in the mitotic entry network. J Cell Biol. 2009;185(2):193-202. doi:10.1083/jcb.200812045

106.Luzhansky ID, Schwartz AD, Cohen JD, et al. Anomalously diffusing and persistently migrating cells in 2D and 3D culture environments. APL Bioeng. 2018;2(2):026112. Published 2018 Jun 19. doi:10.1063/1.5019196

107.Malthus (1789). An Essay on the Principle of Population.

108.Malumbres M, Sotillo R, Santamaría D, et al. Mammalian cells cycle without the D-type cyclin-dependent kinases Cdk4 and Cdk6. Cell. 2004;118(4):493-504. doi:10.1016/j.cell.2004.08.002

109.Mantzaris NV. From single-cell genetic architecture to cell population dynamics: quantitatively decomposing the effects of different population heterogeneity sources for a genetic network with positive feedback architecture. Biophys J. 2007;92(12):4271-4288. doi:10.1529/biophysj.106.100271

110.Martens L, Monsieur G, Ampe C, Gevaert K, Vandekerckhove J. Cell_motility: a cross-platform, open source application for the study of cell motion paths. BMC Bioinformatics. 2006;7:289. Published 2006 Jun 8. doi:10.1186/1471-2105-7-289

111. Masai H, Arai K. Regulation of DNA replication during the cell cycle: roles of Cdc7 kinase and coupling of replication, recombination, and repair in response to replication fork arrest. IUBMB Life. 2000;49(5):353-364. doi:10.1080/152165400410191

112. Massagué J. G1 cell-cycle control and cancer. Nature. 2004;432(7015):298-306. doi:10.1038/nature03094

113. Masuzzo P, Van Troys M, Ampe C, Martens L. Taking Aim at Moving Targets in Computational Cell Migration. Trends Cell Biol. 2016;26(2):88-110. doi:10.1016/j.tcb.2015.09.003

114. Masuzzo P, Huyck L, Simiczyjew A, Ampe C, Martens L, Van Troys M. An end-to-end software solution for the analysis of high-throughput single-cell migration data. Sci Rep. 2017;7:42383. Published 2017 Feb 13. doi:10.1038/srep42383

115. Milo R. What is the total number of protein molecules per cell volume? A call to rethink some published values. Bioessays. 2013;35(12):1050-1055. doi:10.1002/bies.201300066

116. Mitchison TJ, Cramer LP. Actin-based cell motility and cell locomotion. Cell. 1996;84(3):371-379. doi:10.1016/s0092-8674(00)81281-7

117. Mittnacht S. Control of pRB phosphorylation. Curr Opin Genet Dev. 1998;8(1):21-27. doi:10.1016/s0959-437x(98)80057-9

118. Morgan DO. Regulation of the APC and the exit from mitosis. Nat Cell Biol. 1999;1(2):E47-E53. doi:10.1038/10039

119. Morten BC, Scott RJ, Avery-Kiejda KA. Comparison of Three Different Methods for Determining Cell Proliferation in Breast Cancer Cell Lines. J Vis Exp. 2016;(115):54350. Published 2016 Sep 3. doi:10.3791/54350

120. Muinonen-Martin AJ, Veltman DM, Kalna G, Insall RH. An improved chamber for direct visualisation of chemotaxis. PLoS One. 2010;5(12):e15309. Published 2010 Dec 14. doi:10.1371/journal.pone.0015309

121. Nelson RD, Quie PG, Simmons RL. Chemotaxis under agarose: a new and simple method for measuring chemotaxis and spontaneous migration of human polymorphonuclear leukocytes and monocytes. J Immunol. 1975;115(6):1650-1656.

122. Yannis Nevers, Natasha Glover, Christophe Dessimoz, Odile Lecompte, Protein length distribution is remarkably consistent across Life, bioRxiv 2021.12.03.470944; doi: https://doi.org/10.1101/2021.12.03.470944

123. Norman, L. L., Brugués, J., Sengupta, K., Sens, P., & Aranda-Espinoza, H. (2010). Cell blebbing and membrane area homeostasis in spreading and retracting cells. Biophysical journal, 99(6), 1726–1733. https://doi.org/10.1016/j.bpj.2010.07.031

124. Novak B, Tyson JJ. Numerical analysis of a comprehensive model of M-phase control in Xenopus oocyte extracts and intact embryos. J Cell Sci. 1993;106 (Pt 4):1153-1168. doi:10.1242/jcs.106.4.1153

125. Novák B, Tyson JJ. A model for restriction point control of the mammalian cell cycle. J Theor Biol. 2004;230(4):563-579. doi:10.1016/j.jtbi.2004.04.039

126. Okegawa T, Pong RC, Li Y, Hsieh JT. The role of cell adhesion molecule in cancer progression and its application in cancer therapy. Acta Biochim Pol. 2004;51(2):445-457.

127. Ovejero S, Ayala P, Bueno A, Sacristán MP. Human Cdc14A regulates Wee1 stability by counteracting CDK-mediated phosphorylation. Mol Biol Cell. 2012;23(23):4515-4525. doi:10.1091/mbc.E12-04-0260

128. Palecek, S., Loftus, J., Ginsberg, M. et al. Integrin-ligand binding properties govern cell migration speed through cell-substratum adhesiveness. Nature 385, 537–540 (1997). https://doi.org/10.1038/385537a0

129. Pardee AB. A restriction point for control of normal animal cell proliferation. Proc Natl Acad Sci U S A. 1974;71(4):1286-1290. doi:10.1073/pnas.71.4.1286

130. Pardee AB. G1 events and regulation of cell proliferation. Science. 1989;246(4930):603-608. doi:10.1126/science.2683075

131. Park K, Millet LJ, Kim N, et al. Measurement of adherent cell mass and growth. Proc Natl Acad Sci U S A. 2010;107(48):20691-20696. doi:10.1073/pnas.1011365107

132. Perinpanayagam H, Zaharias R, Stanford C, Brand R, Keller J, Schneider G. Early cell adhesion events differ between osteoporotic and non-osteoporotic osteoblasts. J Orthop Res. 2001;19(6):993-1000. doi:10.1016/S0736-0266(01)00045-6

133. Steven Piantadosi, Jane B. Hazelrig, Malcolm E. Turner, A model of tumor growth based on cell cycle kinetics, Mathematical Biosciences, Volume 66, Issue 2, 1983, Pages 283-306, ISSN 0025-5564, https://doi.org/10.1016/0025-5564(83)90094-9.

134. Pietuch A, Janshoff A. Mechanics of spreading cells probed by atomic force microscopy. Open Biol. 2013;3(7):130084. Published 2013 Jul 17. doi:10.1098/rsob.130084

135. Pijuan J, Barceló C, Moreno DF, et al. In vitro Cell Migration, Invasion, and Adhesion Assays: From Cell Imaging to Data Analysis. Front Cell Dev Biol. 2019;7:107. Published 2019 Jun 14. doi:10.3389/fcell.2019.00107

136. Pines, Jonathon. "Cubism and the cell cycle: the many faces of the APC/C." Nature reviews. Molecular cell biology vol. 12,7 427-38. 2 Jun. 2011, doi:10.1038/nrm3132

137. Planas-Silva MD, Weinberg RA. The restriction point and control of cell proliferation. Curr Opin Cell Biol. 1997;9(6):768-772. doi:10.1016/s0955-0674(97)80076-2

138. Pollard TD, Borisy GG. Cellular motility driven by assembly and disassembly of actin filaments [published correction appears in Cell. 2003 May 16;113(4):549]. Cell. 2003;112(4):453-465. doi:10.1016/s0092-8674(03)00120-x

139. Potapova TA, Sivakumar S, Flynn JN, Li R, Gorbsky GJ. Mitotic progression becomes irreversible in prometaphase and collapses when Wee1 and Cdc25 are inhibited. Mol Biol Cell. 2011;22(8):1191-1206. doi:10.1091/mbc.E10-07-0599

140. Pujic Z, Mortimer D, Feldner J, Goodhill GJ. Assays for eukaryotic cell chemotaxis. Comb Chem High Throughput Screen. 2009;12(6):580-588. doi:10.2174/138620709788681952

141. Qu Z, Weiss JN, MacLellan WR. Regulation of the mammalian cell cycle: a model of the G1-to-S transition. Am J Physiol Cell Physiol. 2003;284(2):C349-C364. doi:10.1152/ajpcell.00066.2002

142. Quent VM, Loessner D, Friis T, Reichert JC, Hutmacher DW. Discrepancies between metabolic activity and DNA content as tool to assess cell proliferation in cancer research. J Cell Mol Med. 2010;14(4):1003-1013. doi:10.1111/j.1582-4934.2010.01013.x

143. Raveh A, Margaliot M, Sontag ED, Tuller T. A model for competition for ribosomes in the cell. J R Soc Interface. 2016;13(116):20151062. doi:10.1098/rsif.2015.1062

144. F. J. RICHARDS, A Flexible Growth Function for Empirical Use, Journal of Experimental Botany, Volume 10, Issue 2, June 1959, Pages 290–301, https://doi.org/10.1093/jxb/10.2.290

145. Riveline D, Zamir E, Balaban NQ, et al. Focal contacts as mechanosensors: externally applied local mechanical force induces growth of focal contacts by an mDia1-dependent and ROCK-independent mechanism. J Cell Biol. 2001;153(6):1175-1186. doi:10.1083/jcb.153.6.1175

146. Rossen NS, Hansen AJ, Selhuber-Unkel C, Oddershede LB. Arachidonic acid randomizes endothelial cell motion and regulates adhesion and migration. PLoS One. 2011;6(9):e25196. doi:10.1371/journal.pone.0025196

147. Sacan A, Ferhatosmanoglu H, Coskun H. CellTrack: an open-source software for cell tracking and motility analysis. Bioinformatics. 2008;24(14):1647-1649. doi:10.1093/bioinformatics/btn247

148. Saldivar JC, Hamperl S, Bocek MJ, et al. An intrinsic S/G2 checkpoint enforced by ATR. Science. 2018;361(6404):806-810. doi:10.1126/science.aap9346

149. Salic A, Mitchison TJ. A chemical method for fast and sensitive detection of DNA synthesis in vivo. Proc Natl Acad Sci U S A. 2008;105(7):2415-2420. doi:10.1073/pnas.0712168105

150. Samson SC, Khan AM, Mendoza MC. ERK signaling for cell migration and invasion. Front Mol Biosci. 2022;9:998475. Published 2022 Oct 3. doi:10.3389/fmolb.2022.998475

151. Sagvolden G, Giaever I, Pettersen EO, Feder J. Cell adhesion force microscopy. Proc Natl Acad Sci U S A. 1999;96(2):471-476. doi:10.1073/pnas.96.2.471

152. Schmoller KM, Skotheim JM. The Biosynthetic Basis of Cell Size Control. Trends Cell Biol. 2015;25(12):793-802. doi:10.1016/j.tcb.2015.10.006

153. Schwanhäusser, B., Busse, D., Li, N., Dittmar, G., Schuchhardt, J., Wolf, J., Chen, W., & Selbach, M. (2011). Global quantification of mammalian gene expression control. Nature, 473(7347), 337–342. https://doi.org/10.1038/nature10098

154. Selmeczi D, Mosler S, Hagedorn PH, Larsen NB, Flyvbjerg H. Cell motility as persistent random motion: theories from experiments. Biophys J. 2005;89(2):912-931. doi:10.1529/biophysj.105.061150

155. Sepe L, Ferrari MC, Cantarella C, Fioretti F, Paolella G. Ras activated ERK and PI3K pathways differentially affect directional movement of cultured fibroblasts. Cell Physiol Biochem. 2013;31(1):123-142. doi:10.1159/000343355

156.Serhan CN, Savill J. Resolution of inflammation: the beginning programs the end. Nat Immunol. 2005;6(12):1191-1197. doi:10.1038/ni1276

157.Sha W, Moore J, Chen K, et al. Hysteresis drives cell-cycle transitions in Xenopus laevis egg extracts. Proc Natl Acad Sci U S A. 2003;100(3):975-980. doi:10.1073/pnas.0235349100

158.Shapiro E, Biezuner T, Linnarsson S. Single-cell sequencing-based technologies will revolutionize whole-organism science. Nat Rev Genet. 2013;14(9):618-630. doi:10.1038/nrg3542

159.Sheaff RJ, Groudine M, Gordon M, Roberts JM, Clurman BE. Cyclin E-CDK2 is a regulator of p27Kip1. Genes Dev. 1997;11(11):1464-1478. doi:10.1101/gad.11.11.1464

160.Sherr CJ. D-type cyclins. Trends Biochem Sci. 1995;20(5):187-190. doi:10.1016/s0968-0004(00)89005-2

161.Sherr CJ. Cancer cell cycles. Science. 1996;274(5293):1672-1677. doi:10.1126/science.274.5293.1672

162.Sherr CJ, Roberts JM. CDK inhibitors: positive and negative regulators of G1-phase progression. Genes Dev. 1999;13(12):1501-1512. doi:10.1101/gad.13.12.1501

163.Shimono H, Kaida A, Homma H, Nojima H, Onozato Y, Harada H, Miura M. Fluctuation in radioresponse of HeLa cells during the cell cycle evaluated based on micronucleus frequency. Sci Rep. 2020 Nov 30;10(1):20873. doi: 10.1038/s41598-020-77969-0. PMID: 33257719; PMCID: PMC7705701.

164.Shin S, Dimitri CA, Yoon SO, Dowdle W, Blenis J. ERK2 but not ERK1 induces epithelial-to-mesenchymal transformation via DEF motif-dependent signaling events. Mol Cell. 2010;38(1):114-127. doi:10.1016/j.molcel.2010.02.020

165.Shu KX, Li B, Wu LX. The p53 network: p53 and its downstream genes. Colloids Surf B Biointerfaces. 2007;55(1):10-18. doi:10.1016/j.colsurfb.2006.11.003

166.Sible JC, Tyson JJ. Mathematical modeling as a tool for investigating cell cycle control networks. Methods. 2007;41(2):238-247. doi:10.1016/j.ymeth.2006.08.003

167.Simon SI, Green CE. Molecular mechanics and dynamics of leukocyte recruitment during inflammation. Annu Rev Biomed Eng. 2005;7:151-185. doi:10.1146/annurev.bioeng.7.060804.100423

168. Singh J, Padgett RA. Rates of in situ transcription and splicing in large human genes. Nat Struct Mol Biol. 2009;16(11):1128-1133. doi:10.1038/nsmb.1666

169. Soifer I, Robert L, Amir A. Single-Cell Analysis of Growth in Budding Yeast and Bacteria Reveals a Common Size Regulation Strategy. Curr Biol. 2016;26(3):356-361. doi:10.1016/j.cub.2015.11.067

170. Son, Sungmin et al. "Cooperative nutrient accumulation sustains growth of mammalian cells." *Scientific reports* vol. 5 17401. 1 Dec. 2015, doi:10.1038/srep17401

171. Stähle M, Veit C, Bachfischer U, et al. Mechanisms in LPA-induced tumor cell migration: critical role of phosphorylated ERK. J Cell Sci. 2003;116(Pt 18):3835-3846. doi:10.1242/jcs.00679

172. Swat M, Kel A, Herzel H. Bifurcation analysis of the regulatory modules of the mammalian G1/S transition. Bioinformatics. 2004;20(10):1506-1511. doi:10.1093/bioinformatics/bth110

173. Szekanecz Z, Koch AE. Cell-cell interactions in synovitis. Endothelial cells and immune cell migration. *Arthritis Res*. 2000;2(5):368-373. doi:10.1186/ar114

174. Taheri-Araghi, Sattar et al. "Cell-size control and homeostasis in bacteria." *Current biology : CB* vol. 25,3 (2015): 385-391. doi:10.1016/j.cub.2014.12.009

175. Tanimura S, Chatani Y, Hoshino R, et al. Activation of the 41/43 kDa mitogen-activated protein kinase signaling pathway is required for hepatocyte growth factor-induced cell scattering. Oncogene. 1998;17(1):57-65. doi:10.1038/sj.onc.1201905

176. Tashima, Y., Hanai, T., Hamada, H., Okamoto, M., 2004. Simulation for detailed mathematical model of G1-to-S cell cycle phase transition. Genome Inform. 9.

177. Terhune SS, Jung Y, Cataldo KM, Dash RK. Network mechanisms and dysfunction within an integrated computational model of progression through mitosis in the human cell cycle. PLoS Comput Biol. 2020;16(4):e1007733. Published 2020 Apr 6. doi:10.1371/journal.pcbi.1007733

178. Traynor D, Kay RR. Possible roles of the endocytic cycle in cell motility. J Cell Sci. 2007;120(Pt 14):2318-2327. doi:10.1242/jcs.007732

179. TODARO GJ, GREEN H. Quantitative studies of the growth of mouse embryo cells in culture and their development into established lines. J Cell Biol. 1963;17(2):299-313. doi:10.1083/jcb.17.2.299

180. Toetsch S, Olwell P, Prina-Mello A, Volkov Y. The evolution of chemotaxis assays from static models to physiologically relevant platforms. Integr Biol (Camb). 2009;1(2):170-181. doi:10.1039/b814567a

181. Toscano E, Sepe L, Del Giudice G, Tufano R, Paolella G. A three component model for superdiffusive motion effectively describes migration of eukaryotic cells moving freely or under a directional stimulus. PLoS One. 2022;17(8):e0272259. Published 2022 Aug 2. doi:10.1371/journal.pone.0272259

182. Tyson JJ. Modeling the cell division cycle: cdc2 and cyclin interactions. Proc Natl Acad Sci U S A. 1991;88(16):7328-7332. doi:10.1073/pnas.88.16.7328

183. Verdugo A, Vinod PK, Tyson JJ, Novak B. Molecular mechanisms creating bistable switches at cell cycle transitions. Open Biol. 2013;3(3):120179. Published 2013 Mar 13. doi:10.1098/rsob.120179

184. Varsano G, Wang Y, Wu M. Probing Mammalian Cell Size Homeostasis by Channel-Assisted Cell Reshaping. Cell Rep. 2017;20(2):397-410. doi:10.1016/j.celrep.2017.06.057

185. Verhulst PF: A note on population growth. Correspondence Mathematiques et Physiques 1838, 10:113-121.

186. Vlach J, Hennecke S, Amati B. Phosphorylation-dependent degradation of the cyclin-dependent kinase inhibitor p27. EMBO J. 1997;16(17):5334-5344. doi:10.1093/emboj/16.17.5334

187. Wang HB, Dembo M, Hanks SK, Wang Y. Focal adhesion kinase is involved in mechanosensing during fibroblast migration. Proc Natl Acad Sci U S A. 2001;98(20):11295-11300. doi:10.1073/pnas.201201198

188. Webb DJ, Nguyen DH, Gonias SL. Extracellular signal-regulated kinase functions in the urokinase receptor-dependent pathway by which neutralization of low density lipoprotein receptor-related protein promotes fibrosarcoma cell migration and matrigel invasion. J Cell Sci. 2000;113 (Pt 1):123-134. doi:10.1242/jcs.113.1.123

189. Weibull W: A statistical distribution function of wide applicability. J of Appl Mech 1951, 18:293-297.

190. Weinberg RA. The retinoblastoma protein and cell cycle control. Cell. 1995;81(3):323-330. doi:10.1016/0092-8674(95)90385-2

191. Wessels D, Kuhl S, Soll DR. 2D and 3D quantitative analysis of cell motility and cytoskeletal dynamics. Methods Mol Biol. 2009;586:315-335. doi:10.1007/978-1-60761-376-3_18

192. White RJ. Regulation of RNA polymerases I and III by the retinoblastoma protein: a mechanism for growth control?. Trends Biochem Sci. 1997;22(3):77-80. doi:10.1016/s0968-0004(96)10067-0

193. Inge M.N. Wortel, Annie Y. Liu, Katharina Dannenberg, Jeffrey C. Berry, Mark J. Miller, Johannes Textor, CelltrackR: An R package for fast and flexible analysis of immune cell migration data, ImmunoInformatics, Volumes 1–2, 2021, 100003, ISSN 2667-1190, https://doi.org/10.1016/j.immuno.2021.100003.

194. Wu Q, Kim YC, Lu J, et al. Poly A- transcripts expressed in HeLa cells. PLoS One. 2008;3(7):e2803. Published 2008 Jul 30. doi:10.1371/journal.pone.0002803

195. Xu L, Chen H, Hu X, Zhang R, Zhang Z, Luo ZW. Average gene length is highly conserved in prokaryotes and eukaryotes and diverges only between the two kingdoms. Mol Biol Evol. 2006;23(6):1107-1108. doi:10.1093/molbev/msk019

196. Yang E, van Nimwegen E, Zavolan M, Rajewsky N, Schroeder M, Magnasco M, Darnell JE Jr. Decay rates of human mRNAs: correlation with functional characteristics and sequence attributes. Genome Res. 2003 Aug;13(8):1863-72. doi: 10.1101/gr.1272403. PMID: 12902380; PMCID: PMC403777.

197. Yao G, Lee TJ, Mori S, Nevins JR, You L. A bistable Rb-E2F switch underlies the restriction point. Nat Cell Biol. 2008;10(4):476-482. doi:10.1038/ncb1711

198. Yu FB, Willis L, Chau RM, et al. Long-term microfluidic tracking of coccoid cyanobacterial cells reveals robust control of division timing. BMC Biol. 2017;15(1):11. Published 2017 Feb 14. doi:10.1186/s12915-016-0344-4

199. Zachariae W, Nasmyth K. Whose end is destruction: cell division and the anaphase-promoting complex. Genes Dev. 1999;13(16):2039-2058. doi:10.1101/gad.13.16.2039

200. Zatulovskiy E, Zhang S, Berenson DF, Topacio BR, Skotheim JM. Cell growth dilutes the cell cycle inhibitor Rb to trigger cell division. Science. 2020;369(6502):466-471. doi:10.1126/science.aaz6213

201. Zengel P, Nguyen-Hoang A, Schildhammer C, Zantl R, Kahl V, Horn E. μ-Slide Chemotaxis: a new chamber for long-term chemotaxis studies. BMC Cell Biol. 2011;12:21. Published 2011 May 18. doi:10.1186/1471-2121-12-21

202. Zhang S, Zatulovskiy E, Arand J, Sage J, Skotheim JM. The cell cycle inhibitor RB is diluted in G1 and contributes to controlling cell size in the mouse liver. Front Cell Dev Biol. 2022;10:965595. Published 2022 Aug 25. doi:10.3389/fcell.2022.965595

203. Zicha D, Dunn GA, Brown AF. A new direct-viewing chemotaxis chamber. J Cell Sci. 1991;99 (Pt 4):769-775. doi:10.1242/jcs.99.4.769

204. Zielke N, Edgar BA. FUCCI sensors: powerful new tools for analysis of cell proliferation. Wiley Interdiscip Rev Dev Biol. 2015;4(5):469-487. doi:10.1002/wdev.189

205. Zigmond SH. Ability of polymorphonuclear leukocytes to orient in gradients of chemotactic factors. J Cell Biol. 1977;75(2 Pt 1):606-616. doi:10.1083/jcb.75.2.606

Web sites

MotoCell - http://motocell.dbbm.unina.it

MtrackJ - http://www.imagescience.org/meijering/software/mtrackj/

R - http://www.r-project.org

Imaris Track - https://imaris.oxinst.com/products/imaris-for-tracking

MetaMorph - https://www.moleculardevices.com/products/cellular-imaging-systems/acquisition-and-analysis-software/metamorph-microscopy#gref

Image-Pro Plus - https://www.mediacy.com/imageproplus

ggplot2 - https://www.rdocumentation.org/packages/ggplot2/versions/3.3.5.

RStudio - https://www.rstudio.com.

Rserve - https://cran.r-project.org/web/packages/Rserve/

php - https://www.php.net/

python - https://www.python.org/

Human assembly and gene annotation - http://www.ensembl.org/Homo_sapiens/Info/Annotation

10. Appendix

10.1. *PhotoCell*: a set of macro tools developed to manage time-lapse acquisitions

In order to support advanced time-lapse acquisitions of long-term cell cultures, *PhotoCell*, a new integrated image acquisition tool, was developed by using the macro programming environment available within Zen Blue software and integrated into it, in order to manage the acquisition of time-lapse image stacks through a Zeiss Cell Observer system, composed by an incubator chamber for maintaining temperature and CO_2 levels, an inverted microscope (Axiovert 200M), and a digital camera attached to it (Fig 34).

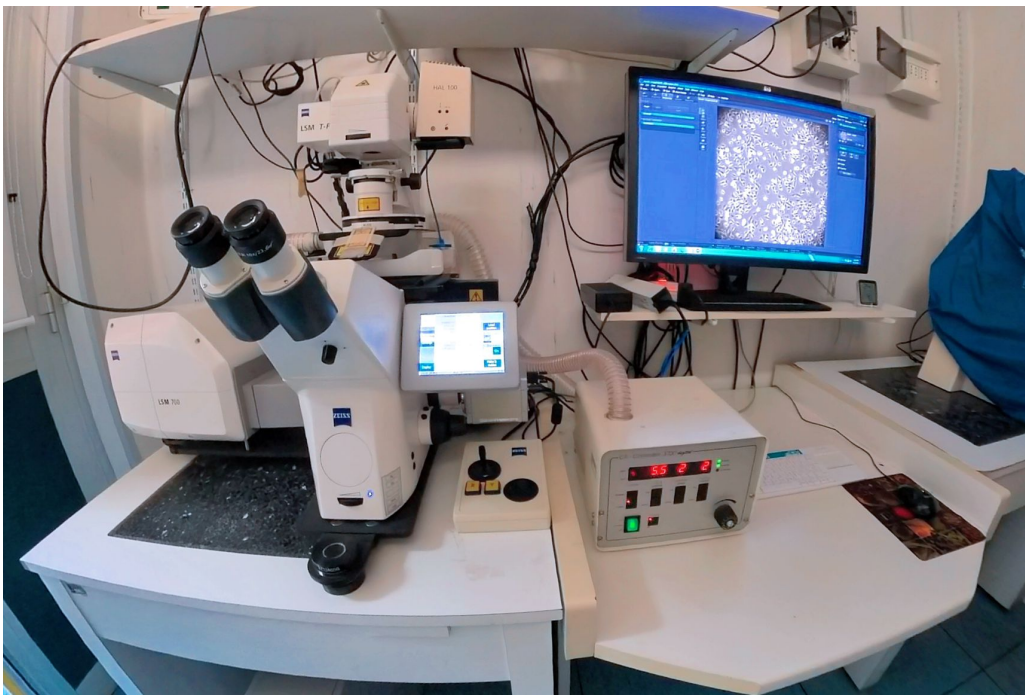

Fig 34. Acquisition observer system. The system consists of Axiovert 200M, an inverted microscope, an incubator chamber associated with systems able to control temperature and CO_2 levels, a digital camera, a computer and a software tool.

The tool introduced into the system, is able to manage the acquisition system and, at the same time, to communicate with a second workstation or a server, dedicated to remotely monitor and save the acquired images (Fig 35). This link allows safe storing and management of all acquisition images and metadata and also an additional way of remote monitoring and controlling the experiment.

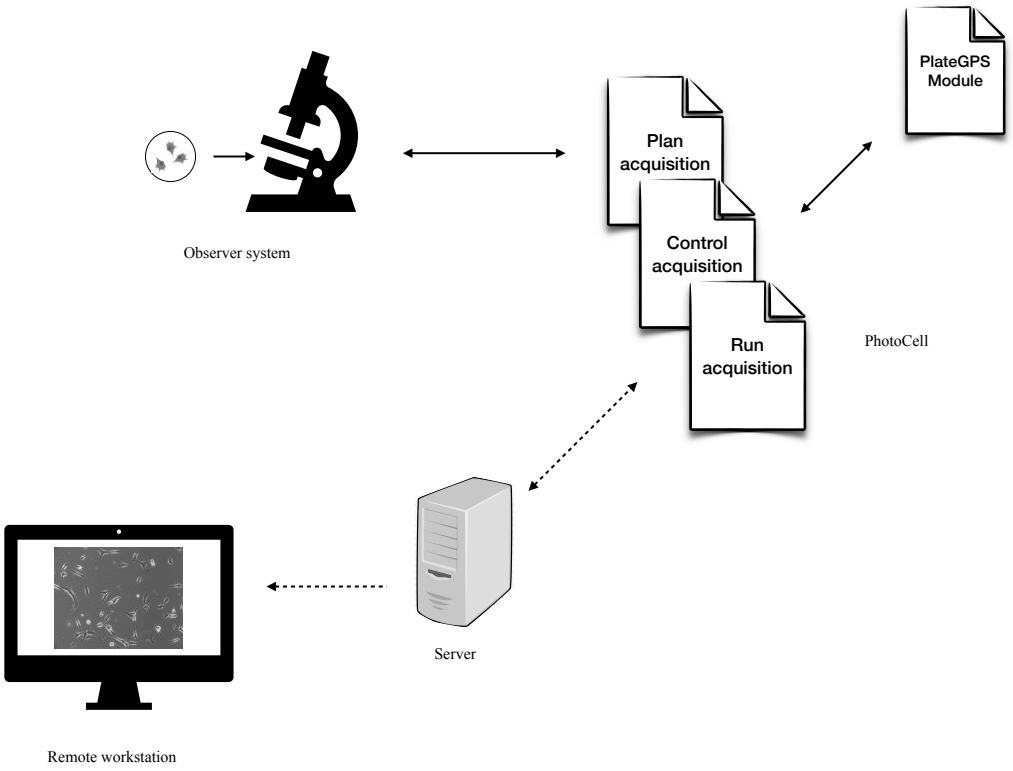

Fig 35. The integrated system for time-lapse acquisitions. *PhotoCell* macros were linked to the observer system, on one side, and a remote server, on the other one.

Photocell was organised as a set of macros, which, taken together, allow to plan customized experiments, control and optionally modify the acquisition settings, before or even while the acquisition is running. This feature is very welcome, as it allows the adjustment of some parameters in reply to changes occurring during the acquisition time, for example focus changes due to mechanical events or cell detachment/attachment. A satellite

module, named plateGPS, was also added to the system to introduce additional functionalities, such as the possibility of calculating and moving to user defined points of a multi-well plate; in this way *PhotoCell* can move the observation point to the centre of a particular well of a plate without manual intervention, even from a remote workstation where no view of the plate is available. The module also provides the ability to calculate and acquire adjacent positions that could be recomposed to produce a final much bigger image.

PhotoCell allows the execution of complex acquisitions, ranging from simple time-lapse experiments to more complex ones lasting for very long times, and sporting high numbers of x-y and/or z-stack positions, essentially limited only by available disk space. It was used to acquire images from a large number of different samples for 24/48 hours or longer periods, and it appears to guarantee accurate time-lapse acquisitions, carefully programmed and in a predictable way, all features which are particularly important when the experiment is aimed to follow a cell culture for an extended period of time. It allows a finer control of the acquisition settings, logs the exact time of each snapshot, and can compensate the effects of a number of unwelcome events, including accidental interruptions due to power failures or network blocks, which would otherwise result in an impaired final acquisition or its loss.